Journal of Energy Chemistry 27 (2018) 1536–1554

Contents lists available at ScienceDirect

Journal of Energy Chemistry

journal homepage: www.elsevier.com/locate/jechem

http://www.journals.elsevier.com/journal-of-energy-chemistry/

Review

The application of nanostructured transition metal sulfides as anodes for lithium ion batteries

Jinbao Zhao*, Yiyong Zhang, Yunhui Wang, He Li, Yueying Peng

State Key Laboratory of Physical Chemistry of Solid Surfaces, State-Province Joint Engineering Laboratory of Power Source Technology for New Energy Vehicle, Collaborative Innovation Center of Chemistry for Energy Materials, College of Chemistry and Chemical Engineering, Xiamen University, Xiamen 361005, Fujian, China

ARTICLE INFO

Article history:
Received 25 December 2017
Revised 9 January 2018
Accepted 10 January 2018
Available online 8 February 2018

Keywords:
Transition metal sulfides
Lithium ion battery
Anode

ABSTRACT

With wide application of electric vehicles and large-scale in energy storage systems, the requirement of secondary batteries with higher power density and better safety gets urgent. Owing to the merits of high theoretical capacity, relatively low cost and suitable discharge voltage, much attention has been paid to the transition metal sulfides. Recently, a large amount of research papers have reported about the application of transition metal sulfides in lithium ion batteries. However, the practical application of transition metal sulfides is still impeded by their fast capacity fading and poor rate performance. More well-focused researches should be operated towards the commercialization of transition metal sulfides in lithium ion batteries. In this review, recent development of using transition metal sulfides such as copper sulfides, molybdenum sulfides, cobalt sulfides, and iron sulfides as electrode materials for lithium ion batteries is presented. In addition, the electrochemical reaction mechanisms and synthetic strategy of transition metal sulfides are briefly summarized. The critical issues, challenges, and perspectives providing a further understanding of the associated electrochemical processes are also discussed.

© 2018 Science Press and Dalian Institute of Chemical Physics, Chinese Academy of Sciences. Published by Elsevier B.V. and Science Press. All rights reserved.



Jinbao Zhao has been engaged in the development and commercialization of chemical power (especially lithium ion batteries) and functional polymer materials, especially in the Japanese Hitachi Group for more than 10 years. He has worked in College of Chemistry and Chemical Engineering, Xiamen University (focusing on lithium-based batteries) since 2011. He is Xiamen University Distinguished Professor, the national "thousands of people plan" distinguished experts and doctoral tutor. His research direction includes: the design, synthesis and industrialization of energy storage materials; the design of high performance lithium ion battery and its electrode; the development of electrolyte and related additive for lithium ion battery; lithium ion battery production process development; large lithium ion battery and new battery system research and development for electric vehicles; fuel cells.



Yiyong Zhang is now a Ph.D. candidate supervised by Prof. Jinbao Zhao in the Department of Chemical and Biological Engineering at the Xiamen University. His research interests are mainly focused on research of transition metal sulfide-based composites for high-performance lithium batteries, positive electrode of lithium sulfur batteries and Si-containing negative electrodes.



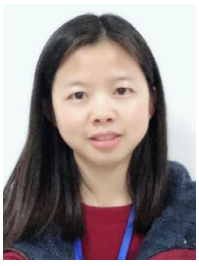
Yunhui Wang is now a Ph.D. candidate supervised by Prof. Jinbao Zhao in the Department of Chemical and Biological Engineering at the Xiamen University. His research interests focus on exploring different design and fabrication methods to prepare transition metal sulfide-based composites for high-performance lithium batteries.

* Corresponding author.
E-mail address: jbzhao@xmu.edu.cn (J. Zhao).

https://doi.org/10.1016/j.jechem.2018.01.009
2095-4956/© 2018 Science Press and Dalian Institute of Chemical Physics, Chinese Academy of Sciences. Published by Elsevier B.V. and Science Press. All rights reserved.



He Li is currently a Ph. D. student under the supervision of Prof. Jinbao Zhao at the State Key Laboratory of Physical Chemistry for Solid Surfaces, Collaborative Innovation Center of Chemistry for Energy Materials, State-Province Joint Engineering Laboratory of Power Source Technology for New Energy Vehicle, and College of Chemistry and Chemical Engineering, Xiamen University. His research interests are fabrications and characterizations of metal chalcogenides and their applications in rechargeable batteries.



Yueying Peng is a Ph.D. student under the supervision of Prof. Jinbao Zhao at College of Chemistry and Chemical Engineering, Xiamen University. Her research interests are mainly focused on lithium-sulfur batteries, including sulfur cathode and lithium sulfide cathode.

1. Introduction

With growing consumption of non-renewable fossil fuels and increasing demand for energy since 1900s, it is an urgent task to explore and develop sustainable energy such as solar, wind, nuclear power. In this regard, the rechargeable battery systems are playing a vital role in the storage of energy harvested from aforementioned renewable power. Since the commercialization of lithium ion batteries (LIBs) in 1991, the LIBs have been widely applied in various electric devices due to the portability, no memory effect, high volume energy density, low self-discharge and long cycle life [1–3]. However, recent emergence of electric vehicles (EVs) and hybrid electric vehicles (HEVs) requests storage systems with higher energy density. The electrochemical performances of batteries have a close relationship with the electrode materials, searching suitable electrode materials has become the key point to improve the energy density of batteries. Ever since the LIBs were commercialized, the commercial graphite has been the prominent choice as the anode material. Although it exhibits many advantages, its shortcomings such as formation of lithium dendrite cannot be neglected, impeding its further application in high-power electric devices. As an alternative to the graphite anode, the $Li_4Ti_5O_{12}$ with high structural stability has been widely investigated. Nevertheless, the low theoretical capacity (~175 mAh g^{-1}) and poor electrical conductivity of $Li_4Ti_5O_{12}$ hinder its widespread use, which is far from the requirement of high energy density in EVs and HEVs. Therefore, it is of significant necessity to exploit and research new-type anode materials.

As one of anode candidates, (de)intercalation/conversion reaction-based transition metal sulfides (TMSs) have drawn growing attention because of their high theoretical capacity, low-cost and environmental-friendliness [4–8]. Compared to the graphite anode, the voltage platform of TMSs is usually above 1.0 V, which avoids the formation of lithium dendrite and ensures the high safety. The theoretical specific capacity and electrical conductivity of TMSs are much higher than those of $Li_4Ti_5O_{12}$. Those attracting advantages show that the TMSs can be the competitive candidates for next-generation anode materials.

Despite these advantages, the strong structural re-organization during (de)lithiation causes large volume change, leading to pulverization and peeling off from the current collector. The loss of active materials and side reactions with electrolytes also deteriorate the performances of TMSs. The poor ionic/electronic conductivity of TMSs, especially for the discharged product (Li_2S), hampered their high-power performances. In order to solve these problems, numerous efforts have been paid and many outstanding works have been reported [5,9]. In this review, we generalize the state-of-art researches and progress of TMSs materials for the LIBs, particularly focus on the discussion about the reaction mechanism, the outline of synthesis methods and their application in LIBs.

2. Characteristic and electrochemical reaction mechanism of TMSs in LIBs

Although the TMSs are known as conversion reaction-based materials, there are still some confusing and disturbing points, especially involving different cut-off voltages. It is different from most oxides that theoretical potentials of electrochemical reactions of most TMSs usually take place above 1.0 V [10]. As anode materials, the capacity of TMSs can be fully released even if the cut-off voltage is set as 1.0 V. In fact, most researchers tend to choose lower cut-off voltage to pursue higher capacity sacrificing the initial Coulombic efficiency (usually below 70%). As we know, there is an intimate connection between the electrochemical properties and material structure. In this section, the lithium storage mechanism of TMSs will be briefly discussed according to the voltage windows (1.0~3.0 V and 0.01~3.0 V).

2.1. Lithium storage mechanism of TMSs between voltage windows of 1.0~3.0 V

Since the (de)intercalation/conversion reaction-based TMSs are mainly discussed here, the discussion of (de)intercalation reaction-based TMSs such as Ti-S, W-S and V-S will be neglected, which can be found in the specialized review [11].

It is well acknowledged that, even for the (de)intercalation/conversion reaction-based TMSs, the lithiation processes are divided into two parts: the (de)intercalation process (Eq. (1)) and the conversion reaction (Eq. (2)).

$$M_aS_b + xLi \rightarrow Li_xM_aS_b \quad (1)$$

$$M_aS_b + 2b\ Li \rightarrow aM + bLi_2S \quad (2)$$

The (de)intercalation process has been proved by many researchers via physical and electrochemical characterization [12–16]. In this process, the transition phases (Li_xMS) are formed with maintaining crystal phase. The capacity in this stage is dependent on the particle size of active material. The particles of smaller size with high specific surface area will provide more (de)intercalation sites, contributing to higher capacity. It is noted that there is a debate about the two-step reaction mechanism of CuS. One argues that the Li_xCuS is formed in the first step while the other proposes that the CuS is reduced to Cu_2S [13,17]. Early in 2002, Chung and Sohn studied the electrochemical behavior (mainly the initial discharge process) of CuS in two different cut-off voltage ranges (1.5~2.6 V and 1.8~2.6 V) via ex-situ XRD method [18]. They pointed out that, between 1.5~2.6 V, the CuS suffers from two-step reduction reactions. The first step happened at about 2.1 V, ascribing to the formation of Li_xCuS intermediate. The other at around 1.7 V belonged to the further reduction of Cu_xS to Li_2S and Cu. The cycling performance of CuS between 1.5 and 2.6 V was dissatisfied because of the irreversible second step reaction, whereas the electrochemical reaction became much more reversible if discharged to 1.8 V. Recently, Kalimuldina and Taniguchi also investigated the behavior of CuS with high phase purity with different current collectors and with/without the interlayer [13]. They found that the severe capacity fading of CuS in the 1st cycle was ascribed to the difficulty in forming high-crystallinity CuS, leading to lose some charge capacity. The following capacity fading was related with the dissolution of unreacted Li_2S_x in the electrolyte. These problems could be well addressed using the current

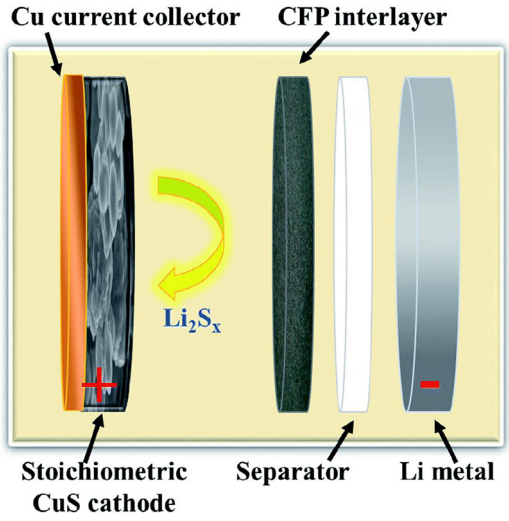


Fig. 1. Schematic illustration of the cell fabrication consisting of stoichiometric CuS cathode electrode coated on a Cu foil current collector, CFP interlayer, separator and lithium metal. Reproduced with permission Ref. [13]. Copyright 2017, Royal Society of Chemistry.

collector and introducing a carbon fiber paper (CFP) as an interlayer (Fig. 1).

Another fantastic TMS is Cu_2S. A pair of flat charge and discharge plateaus can be observed after cycling several cycles. Besides, Cu_2S is more electrochemically stable than that of CuS, as discussed in the mechanism section [13]. The last but not the least, since the ionic radius (0.077 nm) of Cu(I) ion is very close to that (0.076 nm) of Li(I) ion, and the calculated cell volume of Cu_2S ($Fm\bar{3}m$, fcc) is 0.17332 nm^3, which is very close to that (0.18629 nm^3) of Li_2S ($Fm\bar{3}m$, fcc) [21] .The similarity between Cu_2S and Li_2S may give Cu_2S special electrochemical properties such as low volume expansion during charge and discharge (Fig. 2a–2c). Due to the unique electrochemical behavior of copper sulfides, Jache and co-workers proposed that the reaction mechanism of Cu_2S was rather displacement than conventional conversion, as shown in Fig. 2(e) [20]. Using the in-situ TEM technique, McDowell et al. also observed the extrusion of Cu when the cell was fully discharged (Fig. 2f), further confirming the unique electrochemical behavior of Cu_2S compared with its other counterparts [22]. In our previous study, we also demonstrated that adding excess amount of copper was able to significantly improve the cycling stability of copper sulfides despite of the current collector [23]. Another interesting case is MoS_2. Although it belongs to the family of two-dimensional layered materials, it suffers from different lithiation processes, depending on the cut-off voltages. At above 1.8 V, the lithiating intermediate (Li_xMoS_2) forms and the lower discharge plateau at $\sim$ 1.2 V respects the formation of Li_2S and metal Mo, in which the conversion reaction is irreversible [16,24].

Based on the Eq. (2), the theoretical specific capacities of different TMSs can be calculated [10]. Regarding to this process, the conversion reaction seems to be affirmed via in/ex situ TEM/XRD characterization [19,22,25,26]. One of intriguing phenomenon is the formation of Cu dendrite [22]. Rather than the conventional conversion reaction taking place in nano-domains, the behavior of Cu_2S with Li is more like displacement, in which the large copper dendrites surround a Li_2S matrix after fully discharge [19,20]. McDowell et al. considered that this unique extrusion phenomenon would emerge when two requirements were met: (1) a similar structural relationship between initial and final phases to allow a desirable kinetic transformation, (2) fast ion diffusion coefficient in the matrix. In previous study, we analyzed the structural similarity among CuS, Cu_2S and Li_2S, finding that both the space group and cell volume of Cu_2S and Li_2S were surprisingly similar. This similarity may account for the impressive electrochemical performances of Cu_2S [23]. The biggest disadvantage of choosing the narrow voltage window between 1.0 and 3.0 V is the low releasing capacity compared with that of cycling between 0.01 and 3.0 V. However, the decomposition of electrolytes can also be avoided and the high initial Coulombic efficiency is achieved in this voltage window, which is similar with that of Ti-based anode materials [27–30].

2.2. Lithium storage mechanism of TMSs between voltage windows of 0.01∼3.0 V

In most cases, low cut-off voltages such as 0.1 or 0.01 V will be preferably chosen for the TMSs [31–34]. Due to the deep discharge, more capacity can be achieved, especially in the initial discharge. Nevertheless, the inevasible large initial Coulombic inefficiency is also observed [3]. Different from the (dis)charge plateau belonged to conversion reaction at above 1.0 V, the long and sloped plateau is usually considered to be related with: (1) the interfacial charge between metallic nanoparticles and the Li_2S matrix, (2) the decomposition of electrolytes (forming SEI film). This behavior may resemble those of metal oxides behaving at low voltage [35–37]. The initial Coulombic efficiency is relatively low (usually lower than 70%), which has become one of greatest problems hindering the practical application. About the electrochemical behaviors at the low voltage, there is lack of sufficient and systematic study, which deserves to draw on researches of TMSs.

3. Synthesis strategies for TMSs

3.1. Hydro/solvothermal methods

The hydro/solvothermal methods can be defined as a synthetic method of crystals that depends on the solubility of minerals in hot water/solvent under high pressure. Owing to the advantage of cost-efficient and environmentally friendly, the hydrothermal or solvothermal methods have been intensively investigated. In general, the materials synthesized by hydro/solvothermal methods manifest the features of high crystallinity, high phase purity, narrow particle size distributions, controllable size and morphology etc. For example, MoS_2 nanoflowers, MoS_2 microspheres, MoS_2 nanoflakes, MoS_2 nanoplates, MoS_2/C, MoS_2 nanosheets/CNT and MoS_2/graphene composites have been successfully prepared by the hydro/solvothermal methods [38–45].

Yuan et al. [38] applied a hydrothermal route to synthesize 3D flowerlike MoS_2 powders with the assistance of ionic liquid 1–butyl–3-methylimidazolium tetrafluoroborate ([*BMIM*][BF_4]). The MoS_2 nanoflowers showed lithiation/delithiation activity when investigated as anode for LIBs. Feng et al. [39] prepared MoS_2 nanoflakes by a hydrothermal method. The MoS_2 nanoplates were synthesized by a scalable, simple, one-pot reaction using solvothermal method by Hwang et al. [40]. As reported by Ding et al. [41], hierarchical MoS_2 microspheres composed of ultrathin nanosheets were prepared by a hydrothermal method. As-prepared sample exhibited promising lithium storage properties, showing excellent rate capability and cyclic capacity retention. As reported by Wan et al. [42], the hierarchical MoS_2 quasi-hollow microspheres with porous carbon embraced inside, which can also be described as core-shell C@MoS_2 microspheres, were synthesized by a facile hydrothermal methods. As-prepared C@MoS_2 microspheres manifested outstanding cycling performance and rate behavior when used as anode material for lithium-ion batteries. The layered MoS_2/graphene (MoS_2/G) composites were synthesized by an L-cysteine-assisted hydrothermal method, which was reported by Chang and Chen [43].

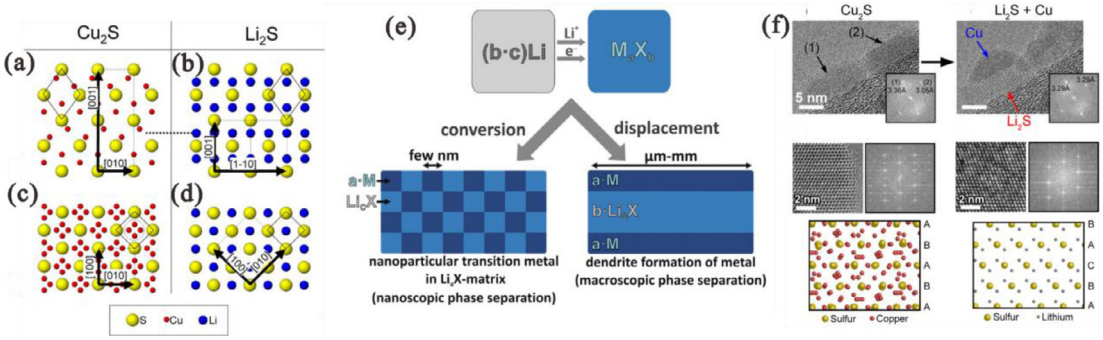


Fig. 2. Structure of Cu_2S along (a) [100] and (c) [001] directions associated, Li_2S structures along (b) [110] and (d) [001] directions. Reproduced with permission Ref. [19]. Copyright 2006, Elsevier. (e) Schematic drawing of the difference between conversion and displacement reactions. Reproduced with permission ref. [20]. Copyright 2014, Elsevier. (f) Transformation of Cu_2S before and after cycling. Reproduced with permission Ref. [22]. Copyright 2015, American Chemical Society.

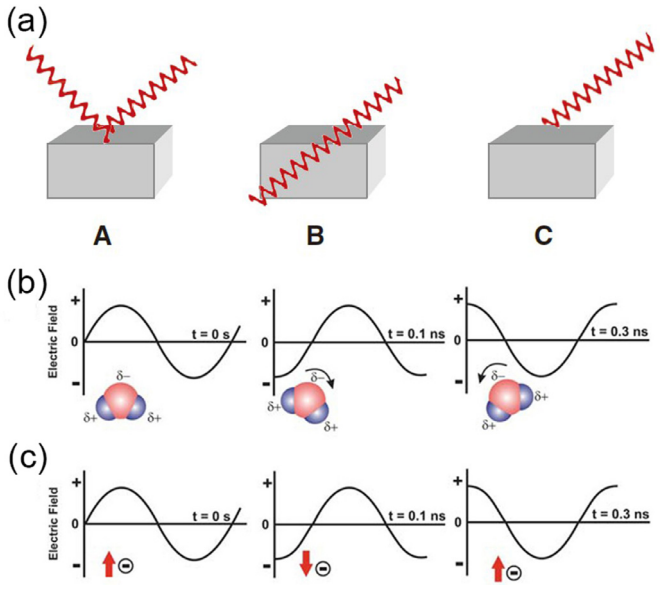


Fig. 3. (a) Microwave interactions with different types of materials: (A) conductive material, (B) insulating material, and (C) absorbing material. Reproduced with permission [46]. Copyright 2014, DeepDyve. Two main heating mechanisms under microwave irradiation: (b) dipolar polarization; (c) ionic conduction mechanism. Reproduced with permission [47]. Copyright 2010, Royal Society of Chemistry.

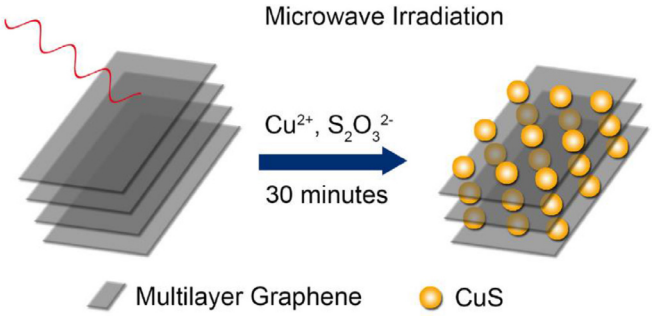


Fig. 4. Schematic illustration of the formation of CuS-G. Reproduced with permission [48]. Copyright 2016, Elsevier.

3.2. Microwave-assisted synthesis

The microwave irradiation is an electromagnetic radiation with the frequency range 0.3~300 GHz, corresponding to wavelengths of 1 mm to 1 m. Microwave-assisted synthesis bases on the efficient heating ability of specific material to absorb microwave energy and to convert microwave energy into heat [46]. The heating mechanism of microwave-assisted synthesis can be summarized into two different processes, namely dipolar polarization and ionic conduction (Fig. 3) [47]. As is often the case, a polar solvent like water, ethanol or acetone is used as the reaction solvent, and the dipolar polarization is the main heating mechanism of microwave-assisted synthesis [47]. The CuS/graphene (CuS-G) composite, binary α-NiS-β-NiS, binder-free CuS, FeS_2 and Ni_3S_2/NiS electrodes, MoS_2/WS_2-rGO composites etc. are rapidly synthesized by the microwave-assisted methods [48–51].

The binary α-NiS-β-NiS has been prepared by a rapid, one-pot microwave-assisted hydrothermal autoclave method within 15 min as reported by Idris et al. [49]. According to Youn et al. [51], the MoS_2/WS_2-rGO composites were fabricated by an ultrafast hybrid microwave annealing method. Xiao et al. [50] reported that the binder-free CuS, NiS/Ni_3S_2, FeS_2 and Co_9S_8 electrodes with various morphologies were in situ synthesized on the according metal foils in the presentence of sulfur by a simple microwave irradiation approach. In the paper of our group, the CuS/graphene (CuS-G) composite was fabricated by one-pot microwave irradiation method under ambient conditions using a domestic microwave oven (Fig. 4) [48].

3.3. Spraying-related methods

The spraying-related methods in this part include the spray pyrolysis, spray deposition and spray drying method. With spray nozzles, the spraying-related methods can spray out liquids and prepare particles efficiently. The spraying-related methods are usually applied to prepare nanostructured metal sulfides with spherical morphology [52]. Up to now, the non-stoichiometric Cu_2S_x, MoS_2/carbon/graphene composite, nickel sulfide and nickel sulfide-carbon composites, WS_2-carbon microspheres and so on have been fabricated successfully by the spray-related methods [44,53–55].

The non-stoichiometric Cu_2S_x has been prepared via a spray pyrolysis method by Kalimuldina and Taniguchi [53]. When the synthetic material was coated on Cu foil current collector, it showed fine cyclic performance and good rate capability. Liu et al. [44] used a hydrothermal approach combined with the spraying coagulation process and calcination step to get composite microspheres consisting of molybdenum disulfide, amorphous carbon, and reduced graphene oxide (MoS_2-AC-rGO). Son et al. [54] prepared nickel sulfide-carbon composites and bare nickel sulfide by one-pot spray pyrolysis method (Fig. 5). In the case of nickel sulfide-carbon composites, a few nanometers the nickel sulfide

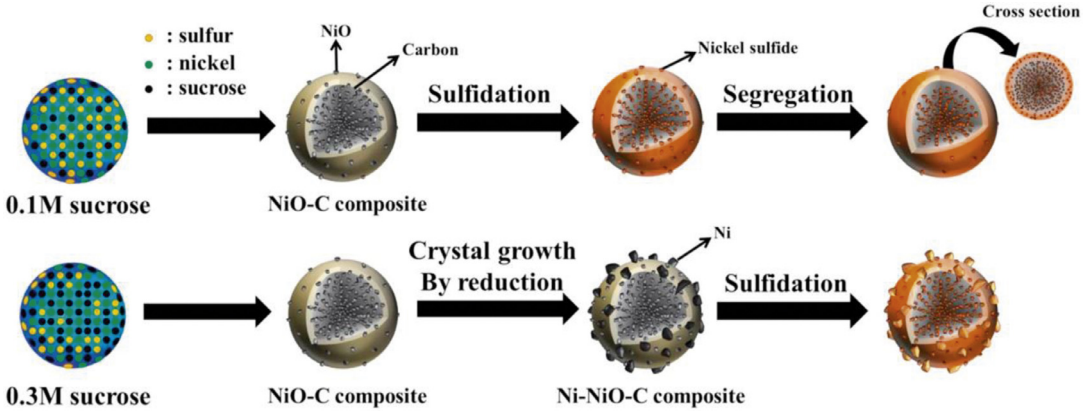


Fig. 5. Mechanisms of formation of the nickel sulfide-carbon composite powders in the spray pyrolysis system [54]. Copyright 2014, Elsevier.

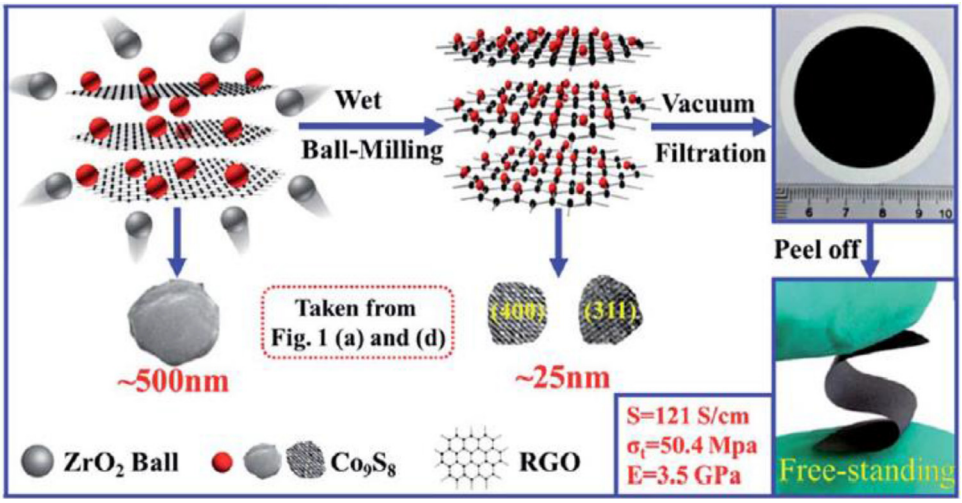


Fig. 6. Schematic illustration of the fabricated flexible and conductive paper using RGO/Co_9S_8. Reproduced with permission [56]. Copyright 2015, Royal Society of Chemistry.

nanocrystals were embraced inside the spherical carbon matrix. The various types of yolk-shell-structured metal sulfide powders can be fabricated by the simple two-step process. The WS_2-carbon composite powders were fabricated by a two-step spray pyrolysis process by Choi et al. [55].

3.4. Other methods

Other methods have also been developed to synthesize metal sulfides. A ball mill is a type of grinder used to grind and blend materials, and the ball milling method can be applied in mineral dressing, paints, ceramics etc. The ball milling owns the strengths of simple raw materials and high efficiency, and it can be used in large scale production. Wang et al. [56] reported a simple high energy ball-milling technique together with vacuum filtration to fabricate a highly flexible, conductive and free-standing rGO/Co_9S_8 nanocomposite paper which could be directly used as a free-standing anode for flexible LIBs (Fig. 6). Han et al. [57] synthesized nickel sulfide by ball milling method. As-prepared material was tested by assembling LIBs, showing fine electrochemical performance. Yersak et al. [58] demonstrated an all-solid-state electrode with a maximum specific energy of 928 Wh kg^{-1}. The active material used in this electrode is FeS_2 made by a ball milling method. The electrospinning is also widely applied to fabricate porous materials with fiber- or tube-like morphologies. Zhu et al. [59] developed a FeS_2@carbon fiber electrode with FeS_2 nanoparticles attached to or embedded in the carbon fibers using an electrospinning method. In the work by Zhang et al. [60], the flexible hybrid membranes with nickel sulfide (NiS) nanoparticles uniformly anchored on the electrospun carbon nanofibers (CNFs) were prepared as binder-free anodes for high-performance LIBs. Through a combination of electrospinning, high-temperature carbonization and the solvothermal reaction, the self-standing membranes of porous carbon nanofiber (PCNF)@MoS_2 core/sheath fibers was facilely obtained, which was reported by Miao et al. [61].

4. TMSs application in LIBs

4.1. Copper sulfides

As the member of TMSs, copper sulfides have been attracting the attentions of researchers. Since copper sulfides contains a series of (non)stoichiometric formulas, CuS and Cu_2S are chosen as the typical copper sulfides in this review to further illustrate the research progress [62].

4.1.1. CuS

Benefiting from the two-electrons electrochemical reaction ($CuS + 2Li^+ + 2e^- \rightarrow Li_2S + Cu$), the theoretical specific capacity of CuS reaches 560 mAh g^{-1}. To improve the electrochemical performance, two kinds of strategies are usually adopted to alleviate the issues such as volume expansion, electronic insulating nature of discharge product (Li_2S): nano-construction and complexing. Constructing nano-structures has been a common way in the

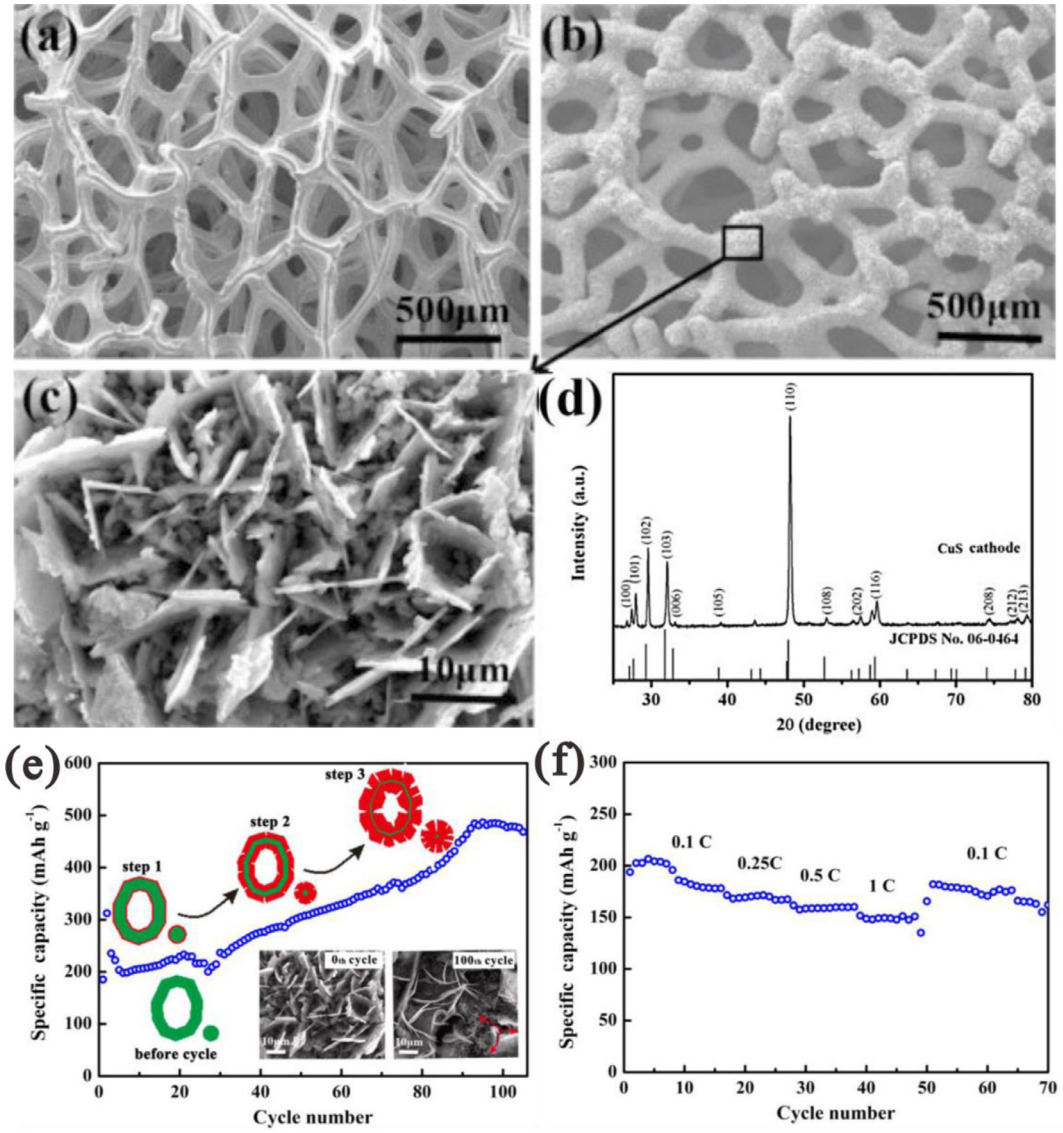


Fig. 7. SEM images of (a) Cu foam, (b, c) hybrid network CuS monolith cathode. (d) XRD pattern of CuS cathode. (e) Cycle performance at 0.2 C (112 mA g^{-1}), along with a proposed schematic diagram of CuS cathode for improving capacity (the insets are SEM images of CuS cathode before cycling and after 100 cycles). (f) Rate capability at different current rates from 0.1 to 1 C. Reproduced with permission [63]. Copyright 2014, Elsevier.

case of (de)intercalation/conversion reaction-based materials since it can effectively address the volume expansion problem. Cheng et al. [63] synthesized hybrid network CuS materials via in situ melt diffusion method. The binder-free CuS cathode showed relatively low initial discharge capacity of 185.1 mAh g^{-1}, whereas a capacity of 468.3 mAh g^{-1} was obtained after 100 cycles. The authors proposed a model to explain that the recovering capacity was related with the stepwise utilization of active material and a reduced dissolution of polysulfides (Fig. 7).

One dimensional nanostructure is another option since it can guarantee desirable electronic conduction along the axial direction and shorter ion diffusion pathway [64,65]. Besides, it allows for better accommodation of volume change during reversible charge and discharge processes [21]. Feng et al. [64] prepared CuS nanowire bundles via a template-free solvothermal method (Fig. 8a). The initial releasing capacity reached 831 mAh g^{-1} at 0.2 C (1 C = 560 mA g^{-1}) with corresponding Coulombic efficiency of 62.3%. After 100 cycles, the reversible capacities were about 570 and 200 mAh g^{-1} at 0.2 and 4 C (Fig. 8b), respectively. Likewise, the CuS nanorod prepared by Li et al. (Fig. 8c) and Zhou et al. (Fig. 8e) also showed excellent cycling stability, as shown in Fig. 8(d) and 8(f) [21,65].

Carbon materials such as carbon nanotube (CNT), graphene, reduced graphene oxide (rGO) are known to exhibit numerous chemical and physical advantages including high electronic conductivity, mechanical strength and structural flexibility [66]. For the metal sulfides suffering from volume change and poor electronic conductivity nature, complexing with carbon materials seems a decent choice to improve the electrochemical performance. Tao et al. [67] obtained CuS/graphene composite via a one-pot hydrothermal method. Compared with the pristine CuS, the CuS/graphene composite showed improved cycling stability and higher reversible capability. At the current density of 50 mA g^{-1}, the composite retained about 296 mAh g^{-1} after 25 cycles, while the capacity of pristine CuS dropped to 50 mAh g^{-1} after 10 cycles. Wang and co-workers [68] successfully prepared the CuS/rGO composite. At 500 mA g^{-1}, the composite showed a reversible capacity of 390 mAh g^{-1} after 200 cycles. Our group [48] also synthesized the CuS/graphene (Fig. 9a and 9b) via a facile microwave-assisted method. The CuS/graphene showed higher reversible

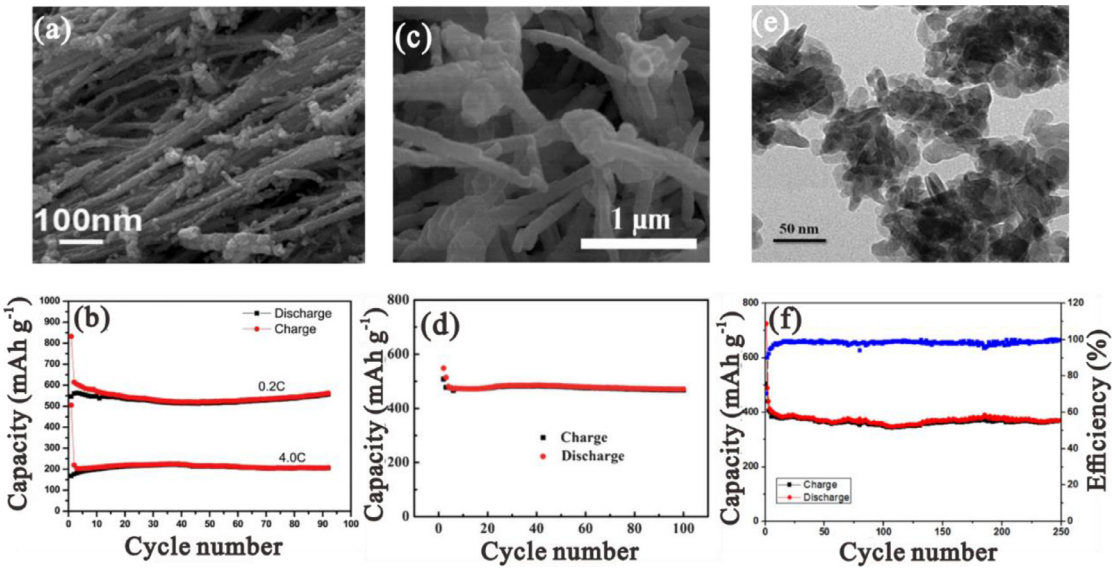


Fig. 8. SEM images of (a) CuS nanowires and (b) corresponding cycling performance at 112 and 2240 mA g^{-1}. Reproduced with permission [64]. Copyright 2014, Elsevier. (c) CuS nanorods and (d) cycling performance at 100 mA g^{-1}. Reproduced with permission [21]. Copyright 2014, Wiley. (e) CuS rod and (f) cycling performance at 112 mA g^{-1}. Reproduced with permission [65]. Copyright 2016, Elsevier.

capacity compared with the pure CuS electrode (Fig. 9c). At the high current density of 2 A g^{-1}, the CuS/graphene remained at 348 mAh g^{-1} after 1000 cycles, displaying excellent cycling stability. Further measurements showed that the introduction of graphene is beneficial to improve the reaction kinetics and to reduce the impedance of cells. Besides introducing graphene-like carbon materials, CNT is regarded as a good conductive network to improve the performance. In our recent work, we prepared 3-dimensional CNTs network/CuS (CuS/CNTs) composite (Fig. 9f) [69]. Through introducing the CNT network, the utilization (Fig. 9g) and the reaction kinetics of CuS were greatly improved, leading to improved cycling stability and rate capability. After 450 cycles, the CuS/0.5CNT released a reversible capacity of 558 mAh g^{-1}, whereas the pristine CuS dropped to 295 mAh g^{-1} at the current density of 400 mA g^{-1} (Fig. 9h).

4.1.2. Cu_2S

Another typical copper sulfide is Cu_2S. The theoretical specific capacity of Cu_2S is 337 mAh g^{-1}, based on one-electron electrochemical reaction. Although showing lower capacity compared with CuS, the Cu_2S still exhibits some fascinating advantages, as previously discussed. To improve the utilization of Cu_2S, similar strategies are adopted. Han et al. [30] in-situ prepared a Cu_2S/tubular mesoporous carbon composite by taking advantage of electrochemical reactions between S C^{-1} composite and a copper foil current collector. After 300 cycles, the composite still released 270 mAh g^{-1} besides the initial Coulombic efficiency of 92%. The authors ascribed the excellent performances to the strong interaction between sulfur and copper ($K_{sp}(Cu_2S) = 1.0 \times 10^{-48}$) (Fig. 10a–10c). Other several groups also prepared Cu_2S/carbon composite to fabricate high-performance anode materials, which showed improved performance compared with the Cu_2S material without any complexing (Fig. 10d–10j) [29,70,71].

Regarding to the copper sulfides, our group is devoting to fabricating high-performance copper sulfide anode materials. For example, a two-step approach has been adopted to prepare Cu_xS/rGO (Fig. 11a and 11b) [72]. Taking advantage of the desirable electronic conductivity and strong mechanical strength of rGO, the problems such as volume expansion and poor electronic conductivity of Li_2S have been well addressed, showing stable cycling performances (Fig. 11c). Further, utilizing the thermally decomposing properties of CuS and thermal stability of coating materials (such as carbon), we deliberately fabricated the $Cu_{2-x}S$@M hollow spheres (Fig. 11d) and the $Cu_{2-x}S$@C bamboo-like hollow nanorods (Fig. 11g) [73,74]. Benefit from the protection of coating shell and internal void space, not only the volume expansion was alleviated, but also the loss of active material during long-term cycling was reduced, guaranteeing excellent cycling stability and rate performances (Fig. 11f and 11i).

4.2. Cobalt sulfides

Different stoichiometric cobalt sulfides (CoS_x) such as Co_9S_8, CoS, Co_3S_4 and CoS_2 have been widely researched because of their excellent physical and chemical properties. The CoS_x [12,75,76] is promising active materials due to their high electrical conductivity, good thermal stability, and high theoretical specific capacities (Co_9S_8: 545 mAh g^{-1}; CoS: 589 mAh g^{-1}; Co_3S_4: 702 mAh g^{-1}; CoS_2: 870 mAh g^{-1}). Among the diverse crystal structures of CoS_x, Co_9S_8, CoS and CoS_2 have been widely studied as anode electrode materials in LIBs. Like the crystal structure of FeS, CoS has a hexagonal in nature with a space group of $P6_3/mmc$ ($a = b = 3.37$ Å and $c = 5.14$ Å) [77]. Thepyrite CoS_2 with a space group of $Pa\bar{3}$ ($a = b = c = 5.53$ Å) is a cubic crystal arrangement, in which the sulfur atoms paired with the Co^{2+} cations in the lattice as S_2^{2-} anions [76]. However, the C_9S_8 is a cubic close-packed arrangement with the $Fm\bar{3}m$ space group ($a = b = c = 9.927$ Å) [78], in which 1/9 of Co atoms are paired with the S octahedral and 8/9 of the Co atoms are coordinated to the S tetrahedron [78–80].

Recently, a large number of studies on the use of Co_9S_8 in LIBs have been reported. In order to improve the conductivity, accommodate the mechanical stress and electrochemical activity of Co_9S_8, the researchers have adopted many strategies. For example, a variety of carbon materials and carbon structures are used to prepare various Co_9S_8 composites, such as Co_9S_8 nanoparticles embedded in threedimensional carbon nanosheet networks [81], graphitic carbon nanocages [82], porous carbon fibers [83], one-dimensional MWCNT [84], yolk-shell carbon sphere and graphene nanosheets [85]. Combining the advantages of carbon materials and carbon structures, the aggregation of Co_9S_8 nanoparticles can be retarded by providing abundant electrochemical active sites and accommodating the mechanical stress during the cycling of LIBs.

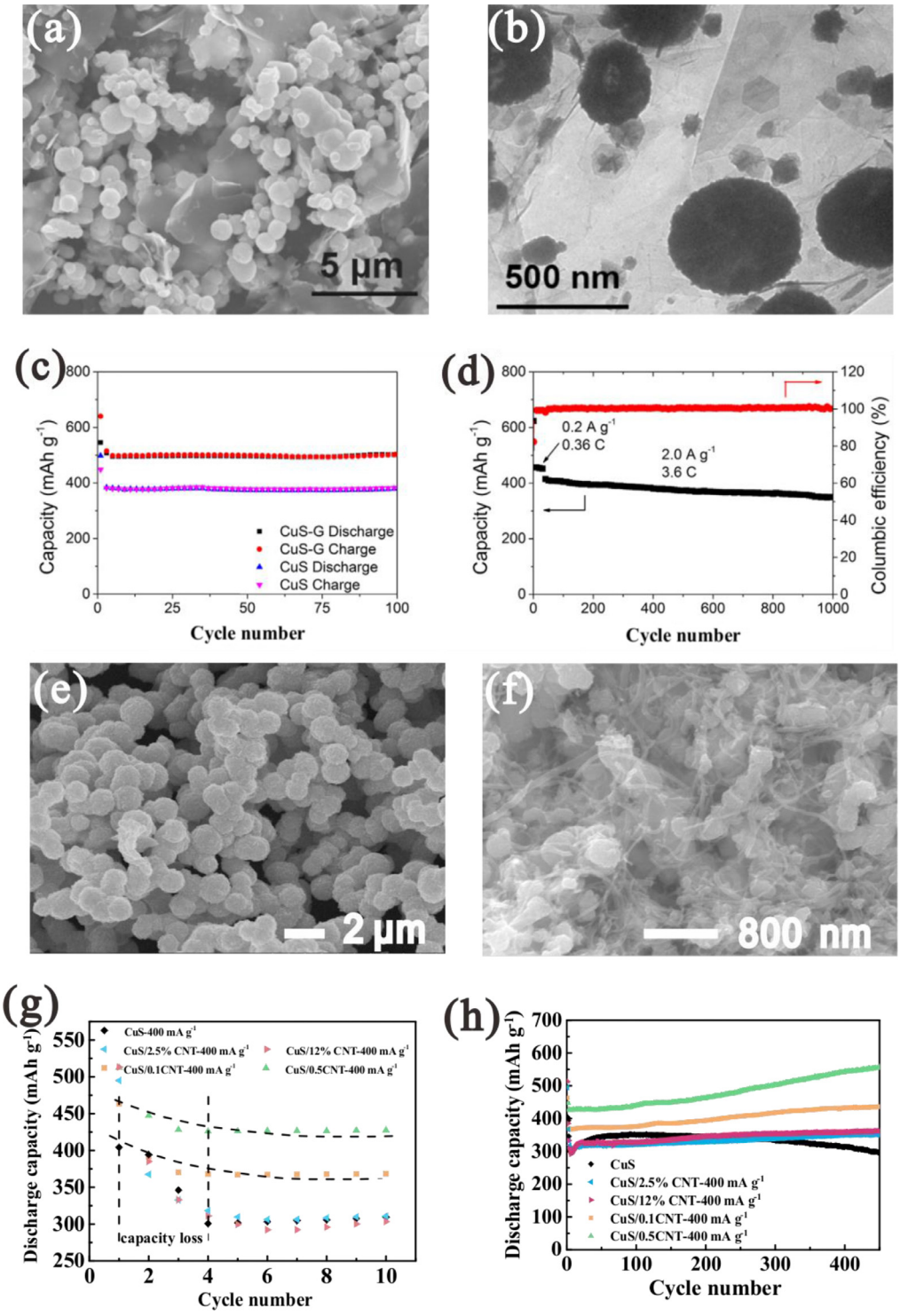


Fig. 9. (a) SEM and (b) TEM images of CuS/graphene. (c) Comparison of cycling performance between pristine CuS and CuS/graphene at 0.2 A g^{-1}, (d) long-term cycling performance of CuS/graphene at 2.0 A g^{-1}. Reproduced with permission [48] Copyright 2017, Elsevier. SEM images of (e) pristine CuS and (f) CuS/0.5CNT composite. (g) Discharge capacities in the first 10 cycles and (h) long-life cycling performances at 400 mA g^{-1}. Reproduced with permission [69] Copyright 2018, Elsevier.

Therefore, when estimated as an anode for LIBs, the as-obtained Co_9S_8 composites electrodes exhibited superior electrochemical performance with a high reversible capacity. For further improve the performance of carbon materials, heteroatoms are doped to carbon materials. For example, Fang et al. [86] used N-rich carbon hollow spheres to build a Co_9S_8 composite material through in situ pyrolysis and sulfurization process. The composites exhibited excellent rate performance. At a current density of 1 C (544 mA g^{-1}), a discharge capacity of 784 mAh g^{-1} was obtained. Even at a current density of 4 C, the composites could still show a discharge capacity of 518 mAh g^{-1}. The excellent rate performance could be attributed to the N-rich carbon encapsulation and the hollow structure.

On the other hand, researchers also designed the structure of Co_9S_8 to improve its performance. Chen's group fabricated polycrystalline rose-like Co_9S_8 hierarchical architectures [80] and

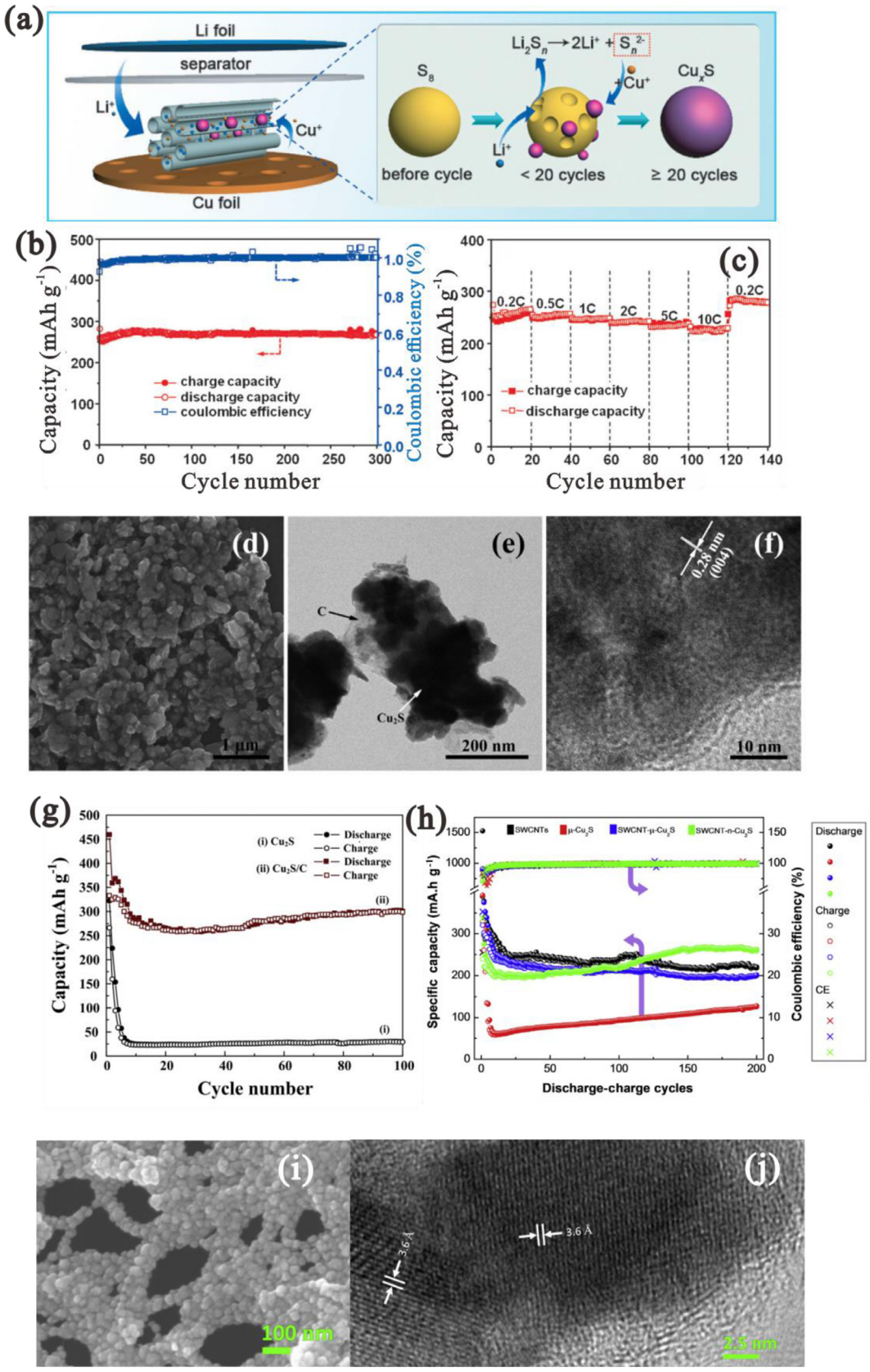


Fig. 10. (a) Schematic of electrode with firmly anchored polysulfide ions, (b) long-term cycling performance and (c) rate capability of Cu_2S/mesoporous carbon composite. Reproduced with permission [30]. Copyright 2014, Wiley. (d) SEM and (e, f) TEM images of Cu_2S/C composite and (g) corresponding cycling performances of Cu_2S and Cu_2S/C composite. Reproduced with permission [70]. Copyright 2015, Elsevier. (h) SEM and (i) TEM images of SWCNT-*n*-Cu_2S and (j) corresponding cycling performances of Cu_2S and Cu_2S/C composite. Reproduced with permission [71]. Copyright 2015, Elsevier.

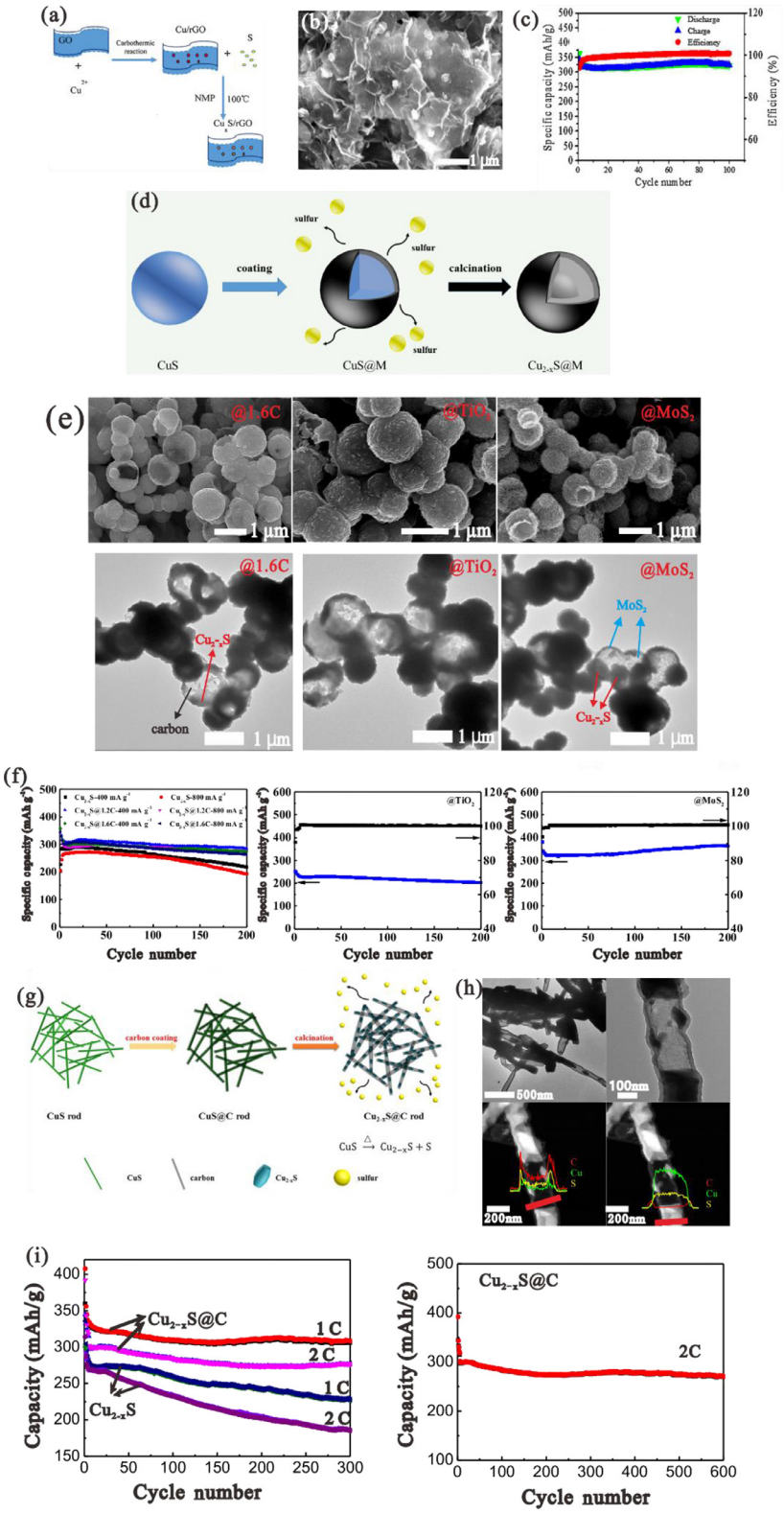


Fig. 11. (a) Synthetic sketch, (b) SEM image and (c) cycling performance of Cu_xS/rGO composite. Reproduced with permission [72]. Copyright 2016, Elsevier. (d) Schematic illustration, (e) morphologies, and (f) cycling performances of $Cu_{2-x}S$@M (M = C, TiO_2 and MoS_2) hollow spheres. Reproduced with permission [73]. Copyright 2017, Springer. (g) Synthetic scheme, (h) TEM images, and (i) cycling performances (1 C = 337 mA g^{-1}) of $Cu_{2-x}S$@C bamboo-like nanorods. Reproduced with permission [74]. Copyright 2017, Elsevier.

mesocrystal Co_9S_8 hollow spheres [87], respectively. These special Co_9S_8 architectures possessed high discharge capacities and good cycling performance as cathode materials for application in LIBs. This is because that such well-defined structure with high surface area can effectively shorten the diffusion path of Li^+ and electrons, leading to delithiation and lithiation very easily during the charge-discharge process, resulting in good Li^+ storage performance. Moreover, Long et al. [88] synthesized two-dimensional Co_9S_8 nanosheets with a thickness of ~10 nm and lateral size of several hundred nanometers and the Co_9S_8 nanoparticles with a diameter of 40 nm. In contrast, the Co_9S_8 nanosheets exhibited cycling stability and enhanced rate capability due to their unique two-dimensional nanostructures. When discharging-charging at 1.0 A g^{-1}, the Co_9S_8 nanosheets showed a reversible capacity as high as 746.8 mAh g^{-1} after 300 cycles, while the Co_9S_8 nanoparticles only delivered 63.6 mAh g^{-1}. Qian et al. [89] successfully fabricated hollow nanospheres of mesoporous Co_9S_8. When discharging-charging at 100 mA g^{-1}, these hollow Co_9S_8 nanoparticles showed a reversible capacity of ~ 1414 mAh g^{-1} after 100 cycles. In order to further improve the reversible capacities at high rates, a carbon shell had grown on the hollow nanospheres. When discharging-charging at 2 A g^{-1}, it showed as high as ~ 896 mAh g^{-1} after 800 cycles.

The CNT-encapsulated TMSs are promising candidates for application as anode materials in LIBs, but their mechanism and electrochemical properties still remain unclear. In order to design and develop high-performance materials of this type of composites, a comprehensive understanding its mechanism at nanoscale of will be must. Therefore, Su et al. [90] investigated the lithium storage mechanism of Co_9S_8/Co nanowire-filled CNTs material by in situ transmission electron microscopy. The study found that for the closed CNT, the lithiation Co_9S_8 nanowire showed a radial expansion of 32.4% and an axial elongation of 4.5%, while the lithiation nanowire core was still confined inside the CNT. Contrastively, for an open CNT, during lithiation, the Co_9S_8 nanowire showed an axial elongation of 94.2% and was squeezed out from the open CNT. Especially, the study found that a thin graphite shell was drawn out from the CNT wall by the squeezed lithiation Co_9S_8. The thin graphite shell confined the squeezed filler and protected the filler from pulverization in the following cycle. During many cycles, the Co segment remained intact while the Co_9S_8 exhibited a reversible transformation between Co nanograins and Co_9S_8. Their observations provided directly mechanism and electrochemical behavior that governed the CNT-based anode performance in LIBs.

Similarly, some studies on the use of CoS in LIBs have been reported. Wang et al. [91] demonstrated a simple and effective solvothermal method to prepare CoS/CNTs nanocomposites, in which CoS nanoparticles coated on the CNTs. When evaluated as anode materials for LIB at the current density of 100 mA g^{-1}, the CoS/CNTs nanocomposites showed excellent cycle stability and kept a high discharge capacity of 780 mAh g^{-1} after 50 cycles. The superior electrochemical performances were ascribed to better electron transportation originated from CNTs and the good combination of the hybrid structure. Likewise, graphene is also used as the framework for fabricated CoS/G composites to solve the agglomeration and electrical conductivity issues of the CoS materials. Furthermore, graphene can also buffer the volume expansion and mitigate pulverization of CoS nanostructures during lithiation and de-lithiation processes. For example, both the CoS/rGO [92] and CoS/GN [93] are reported. They all showed excellent electrochemical performance. When cycling at 100 mA g^{-1}, the CoS/rGO showed a capacity as high as 939 mAh g^{-1} after 100 cycles and remained Coulomb efficiency above 98%. And when charging-discharging at 200 mA g^{-1}, the CoS/GN delivered a reversible capacity as high as 890 mAh g^{-1} without any capacity fading after 80 cycles. Simultaneously, some researches on the use of CoS_2 in LIBs have also been reported. Like other TMSs, limiting CoS_2 to various carbon materials is an effective way to improve its electrochemical performance, such as CNTs [94,95], graphene [94, 96-99] and hollow C microspheres [100–102]. Furthermore, in order to explore the electrochemical behaviors and mechanism of CoS_2 during the charge anddischarge, Su et al. [103] investigated its electrochemical process using in situ transmission electron microscopy. Ultimately, they proposed two mechanisms. As shown in Fig. 12(b), the pure CoS_2 particles exhibited the formation of cracks and fractures due to large and anisotropic size expansion (47.1%) caused by a side-to-side conversion process. Compared the pure CoS_2 particles, the CoS_2 particles anchored on reduced graphene oxide (rGO) sheets showed few fractures due to small and homogeneous size expansion (28.6%) caused by a core-shell conversion process, which was attributed to the superior Li^+ conductivity of rGO and accounted for the enhanced cyclability. After the first discharge, single crystalline CoS_2 particle converted to 1~2 nm Co nanocrystals embedded within Li_2S matrix. The follow cycle was a reversible phase transition between CoS_2 nanocrystals and Co/Li_2S (Fig. 12a).

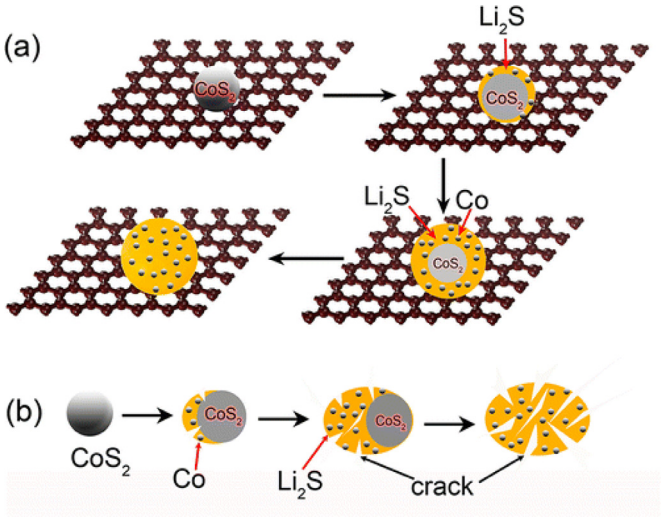


Fig. 12. Schematic drawing showing the electrochemical lithiation process. (a) CoS_2 particles anchored on rGO sheets show a core–shell conversion process; (b) pure CoS_2 particles show a side-to-side conversion process. Reproduced with permission [103]. Copyright 2014, American Chemical Society.

4.3. Molybdenum disulfides

The molybdenum disulfide has a layered structure, where a plane of molybdenum atoms is sandwiched by planes of sulfide ions. The bulk MoS_2 consists of stacked MoS_2 monolayers, which are held together by weak van der Waals force. MoS_2 has been intensively investigated as electrode materials for LIBs because Li^+ ions can easily intercalate/extract from these kinds of layer materials [104,105]. As anode materials for LIBs, the MoS_2 shows many other advantages, for instance, the capacity of MoS_2 (as high as 1300 mAh g^{-1}) is much higher than that of commercial graphite anodes (372 mAh g^{-1}). On the other hand, the MoS_2 generally display better rate performance and low degradation rate compared to other emerging negative electrode materials such as silicon or germanium [106].

The lithium storage property and lithium storage mechanism of commercial bulk MoS_2 were investigated by Fang et al. [107]. It is found out that although the bulk MoS_2 showed outstanding cycling stability in different voltage ranges, the structural transition of bulk MoS_2 in the initial cycling was irreversible. Unlike other metal oxides or sulfides, the metallic Mo as the final production of discharge reaction, was found as electrochemically inert

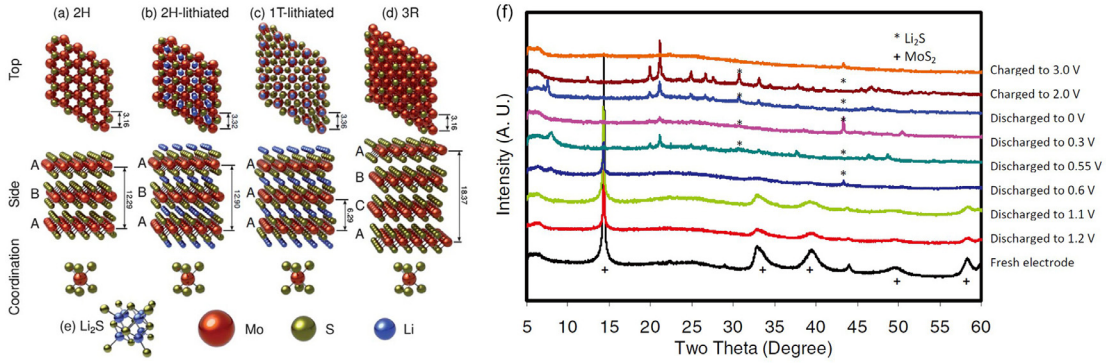


Fig. 13. Molecular models of (a) 2H–MoS_2. (b) Lithiated 2H–MoS_2 showing a 5% lattice expansion in the c-direction and a-direction due to intercalation. (c) Lithiated 1T–MoS_2 showing lithium ions occupying octahedral interstices. (d) 3R–MoS_2, (e) Li_2S (domains of this phase would be interspersed with molybdenum nanoparticles). Dimensions are shown in Angstroms. Reproduced with permission [106]. Copyright 2014, Royal Society of Chemistry. (f) Comparison of MoS_2 electrodes at different DODs and SOCs. Reproduced with permission [112]. Copyright 2011, Wiley-VCH.

and Li_2S/S was the redox couple in a deeply discharged MoS_2/Li battery (0.01 V vs. Li/Li^+) [19,23,108–111]. The metallic Mo did not participate in the subsequent electrochemical lithium storage process. When the MoS_2/Li battery was charged back to 3.0 V, the products were Mo and S instead of MoS_2 (Fig. 13a–e). Xiao et al. [112] reported the ex-situ XRD of MoS_2/Li battery, similar conclusion was drawn that discharge product of metallic Mo is inert and Li_2S/S is the redox couple afterwards (Fig. 13f). After charged to 3.0 V, only the XRD lines of metallic Mo and S could be observed from the XRD pattern. The presence of metallic Mo could help to suppress the dissolution of Li_2S_x which tended to dissolve in the electrolyte and spoilt the cyclic performance. It is well known that the most popular strategy to improve the performance of lithium-sulfur batteries is to encapsulate S into mesopores of carbon or adsorb S on the surface of nanofibers or nanotubes. This strategy can also be applied in the MoS_2/Li battery system. Yu et al. [113] reported a rational design and synthesis of novel nanosheets-on-box nanostructure composed of ultrathin MoS_2 nanosheets on N-doped carbon nanoboxes (C@MoS_2 nanoboxes). The ultrathin MoS_2 nanosheets were stuck on or embedded in the well-defined carbon nanoboxes. Used as anode materials for LIBs, the C@MoS_2 nanoboxes showed outstanding electrochemical performance: these C@MoS_2 nanoboxes manifested high specific capacity of around 1000 mAh g^{-1} at a current density of 0.1 A g^{-1}, excellent cycling stability up to 200 cycles, and fine rate performance. The enhanced lithium storage property was attributed to their unique structure, especially to the high conductivity of N-doped carbon nanoboxes substrate. The hollow structure of carbon nanoboxes effectively relieved the strain caused by large volume change during lithiation. The ultrathin MoS_2 nanosheets possessed high surface area for electrode interface and decreased Li ions diffusion length. All these merits contributed to the electrochemical performance of as-prepared C@MoS_2 nanoboxes. Li et al. [45] prepared MoS_2/graphene hybrid nanoflowers by a simple hydrothermal route. The material characterization showed that the 3D hierarchical composite had large amount of MoS_2 nanopetals with expanded interlayer spacing (Fig. 14). As-prepared composite delivered a reversible capacity of about 1150 mAh g^{-1} at a current density of 100 mA g^{-1}. As a comparison, the pristine MoS_2 and MoS_2–C composite displayed a lower specific capacity and worse cyclic performance. The better performance of MoS_2–C composite was due to 2-dimensional conductive rGO and effective inhibition of the MoS_2 degeneration during lithiation/delithiation process. In addition, the increased layer distance between MoS_2 layers provided sufficient space for Li ions to insert.

Recently, the research has shown that except for composition and arrangement of atoms, the dimensionality also plays an important role in the property and performance of a certain material. Over the past few years, two-dimensional (2D) graphene has been extensively studied. The graphene exhibits unique properties that are absent in bulk graphite, such as mechanical strength, optical properties. The success of graphene sparks the investigation of other 2D materials. Particularly, the 2D transition metal dichalcogenides with layer structures that are similar with graphene have received significant attention. The 2D monolayer or few layer MoS_2 has been studied for energy related applications due to the unique properties of layered structure, including batteries, fuel cells, photoelectrochemistry and so on [114]. And Wang et al. [115] prepared few-layered MoS_2 and covalently sulfur-doped graphene (MoS_2/SG) by a facile solvothermal. The covalent bond of sulfur atoms and graphene sheets effectively bridging 2D few-layered MoS_2 and graphene enable high robustness of the composite materials. Moreover, the compact contact of MoS_2 and highly conductive graphene provided electron transfer pathways through the electrode, while the high surface area allowed fast access to active materials. Such a unique architecture ensured the electrode with the superior cycling stability and excellent rate capability, which was also interpreted by the density functional theory (DFT) calculations. At the current density of 100 mA g^{-1}, an initial discharge capacity of 1670 mAh g^{-1} was obtained with a high initial Coulombic efficiency of 96.5%. After 2000 cycles at a high current density of 10 A g^{-1}, a capacity retention up to 92.3% could be achieved. Even at the current density of 20 A g^{-1}, the MoS_2/SG electrode could still possess a specific capacity of 766 mAh g^{-1}. Jiang et al. [116] synthesized a novel 2D hybrid nanosheet structure consisting of alternatively overlapped single layer MoS_2 and mesoporous carbon with as-made oleic acid (OA) functionalized MoS_2 nanosheet as a template. The ultrathin hierarchical nanosheet structure formed perfect atomic interface contact between single layer MoS_2 and mesoporous carbon sheets, providing enough space and interface area for Li ions to react with MoS_2 (Fig. 15). Compared with the annealed MoS_2 nanosheets (483 mAh g^{-1}), the exfoliated graphene (487 mAh g^{-1}) and the MoS_2/G composites (744 mAh g^{-1}), as-prepared single layer MoS_2-mesoporous carbon nanosheets (MoS_2/m-C) showed much higher capacity (1113 mAh g^{-1}) at 400 mA g^{-1} with excellent rate performance (943 mAh g^{-1} at 6400 mA g^{-1}). Moreover, the MoS_2/m-C nanosheets also exhibited stable cycling performance, where the specific capacity could be well-maintained at 1023 mAh g^{-1} at the current density of 400 mA g^{-1} after 500 cycles. Interestingly, the synthetic material manifested excellent

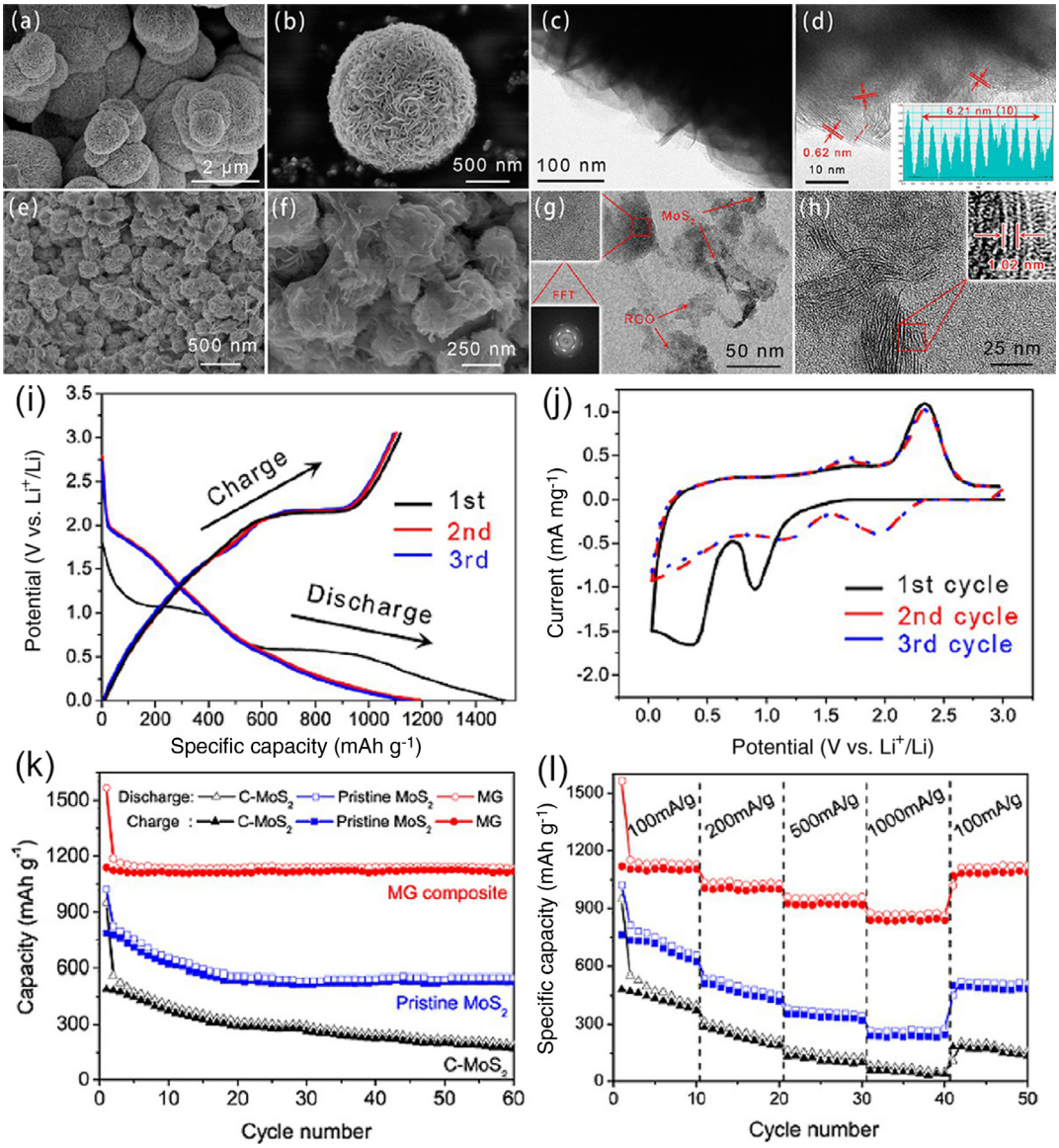


Fig. 14. SEM and TEM images of the pristine MoS_2 and MG composite. (a and b) The SEM images of the pristine MoS_2 in low and high magnifications. (c and d) TEM and HRTEM images of the pristine MoS_2. (e and f) The SEM images of MG composite in low and high magnifications. (g and h) TEM and HRTEM images of MG composite. Inset in (g) is the FFT pattern of the red square obtained from the HRTEM image. (i) First three galvanostatic charge/discharge profiles of MG composite; (j) cyclic voltammograms of MG electrode at a scanning rate of 0.5 mV s^{-1} during the first three cycles; (k) and (l) cycling behaviors and rate capabilities of the three structures: C-MoS_2, pristine MoS_2, and MG composite, respectively. Reproduced with permission [45]. Copyright 2015, American Chemical Society.

capacity, rate ability and excellent cyclic stability at low temperature (3 °C) and high temperature (50 °C). The first-principle DFT calculation of lithium storage on MoS_2/m-C nanosheet structure further supported that there was an enhancement for Li ion intercalation in the MoS_2/G atomic interface system, compared with the separated MoS_2 layer interface. Especially, the MoS_2/m-G interface with a carbon vacancy possessed a more prominent capacity to adsorb Li atoms. The enhancement could be ascribed to the synergetic effect from mesoporous carbon and single-layered MoS_2 nanosheets.

4.4. Iron sulfides

The iron sulfides contain a series of compounds, including stoichiometric FeS, FeS_2 and nonstoichiometric Fe_xS ($1 < x < 2$) and so forth. Among these compounds, the pyrite (cubic-FeS_2) has gained much attention as a promising electrode material for rechargeable LIBs. The pyrite owns the advantages of high theoretical energy density (~ 1313 Wh kg^{-1}), good thermal stability, low cost, earth abundant, nontoxic etc. Compared with other metal sulfides, the pyrite has been applied in Li-FeS_2 primary batteries long and successfully, and it would be more viable to develop commercial FeS_2-based LIBs compared with other metal sulfides [59,117,118].

The charge and discharge mechanism of Li/FeS_2 batteries were studied by in situ X-ray diffraction (XRD) and in situ ^{57}Fe Mössbauer spectroscopy by Fong et al. [119]. It is supposed that the discharge process included a two-step reaction, where the FeS_2 converted into layer structured Li_2FeS_2 firstly, and then the metallic Fe and Li_2S were formed after fully discharge process. In the charge process, however, after the reversible conversion of Li_2FeS_2, a hexagonal $Li_{2-x}FeS_2$ ($0 \le x \le 0.8$) was formed as the intermedia, and then hexagonal $Li_{2-x}FeS_2$ convert into nonstoichiometric pyrrhotite FeS_y and elemental S instead of pyrite FeS_2. The supposed reaction mechanism is listed below:

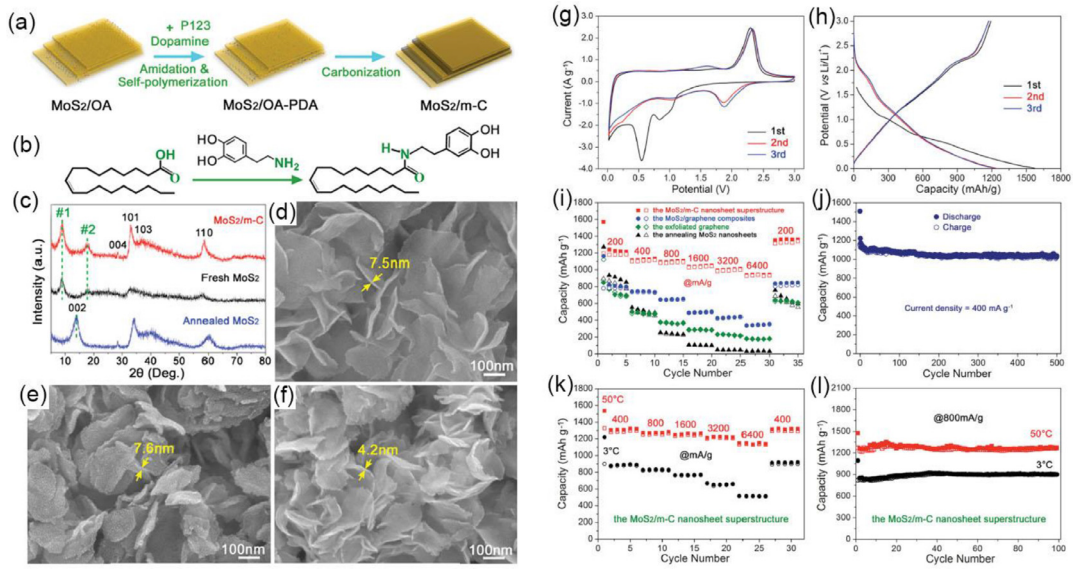


Fig. 15. Synthesis process and morphology characterization. (a) Schematic illustration on the synthesis process of the MoS_2/m-C nanosheet super-structure; (b) the amidation reaction equation of OA and PDA; (c) XRD patterns of the MoS_2/m-C nanosheet superstructure, the fresh MoS_2 nanosheets, and the annealed MoS_2 nanosheets; SEM images of (d) the fresh MoS_2 nanosheets, (e) the MoS_2/m-C nanosheet superstructure, and (f) the annealed MoS_2 nanosheets. Electrochemical and LIB performance: (g) CV curves and (h) charge/discharge curves of the MoS_2/m-C nanosheet superstructure for the first three cycles at 0.2 mV s^{-1}, (i) the capacities retention of the MoS_2/m-C nanosheet superstructure, MoS_2/graphene composites, exfoliated graphene, and the annealed MoS_2 nanosheets at current densities from 200 to 6400 mA g^{-1}, (j) cycling performance of the MoS_2/m-C hybrid nanosheet super-structure at 400 mA g^{-1} for 500 cycles. (k) The capacity retention at different current densities, and (l) cycling stability at 800 mA g^{-1} of the MoS_2/m-C hybrid nanosheet superstructure at low temperature (3 °C) and high temperature (50 °C). Reproduced with permission [116]. Copyright 2015, Wiley-VCH.

Discharge:

$$FeS_2 + 2Li^+ + 2e^- \rightarrow Li_2FeS_2 \quad (3)$$

$$Li_2FeS_2 + 2Li^+ + 2e^- \rightarrow 2Li_2S + Fe \quad (4)$$

Charge:

$$Fe + 2Li_2S \rightarrow Li_2FeS_2 + 2Li^+ + 2e^- \quad (5)$$

$$Li_2FeS_2 \rightarrow Li_{2-x}FeS_2 + xLi^+ + xe^- \quad (6)$$

$$Li_{2-x}FeS_2 \rightarrow FeS_y + (2\text{-}y)S + (2\text{-}x)Li^+ + (2\text{-}x)e^- \quad (7)$$

Similar conclusion is drawn by Zhang and Tran [111], where ex-situ XRD and energy dispersive X-ray (EDX) analysis were conducted to study the reaction mechanism of FeS_2/Li batteries (Fig. 16). Zhang et al. found that during the charge-discharge process, the polysulfides Li_2S_n ($2 \le n \le 8$) were formed and dissolved in the electrolyte. Like lithium-sulfur batteries, the FeS_2/Li batteries would also suffer from so called shuttling effect and cause capacity decline. Certain electrolyte addictive and the coating of active materials could relieve the decay of FeS_2/Li batteries from some extent. Son et al. [120] embed phase pure natural pyrite in a stabilized polyacrylonitrile (PAN) matrix. The PAN matrix could confine FeS_2's electroactive species (Fe^0 and Sn^{2-}) for good reversibility and efficiency. In addition, the PAN matrix could accommodate the 160% volume change during the discharge process because the PAN coating was not fully carbonized. Using high resolution transmission electron microscopy (HRTEM), it was confirmed that the FeS_2 particles were embedded in the PAN matrix and the FeS_2's electroactive species were well confined during cycling. After 50 cycles, the capacity of PAN-FeS_2 electrode maintained at 470 mAh g^{-1} with a Coulombic efficiency up to 99.25%. The core-shell nano-FeS_2@N-doped graphene was prepared by Tan et al. [121]. The nano-sized FeS_2 had a short Li ion diffusion distance, and the N-doped graphene shell had optimized electronic conductivity in addition to mechanical strength that could maintain the structural stability of active materials. As-prepared cells had superior electrochemical performance with a high reversible capacity of 484.7 mAh g^{-1} at 0.5 A g^{-1}, corresponding to a specific energy density of 713.5 Wh kg^{-1}. The FeS_2 cells also exhibited outstanding fast rechargeable performance, at a current density of 5 A g^{-1}, the capacity stood at 281.4 mAh g^{-1} (543 Wh kg^{-1}). Additionally, the cells with core-shell nano-FeS_2@N-doped graphene electrode had excellent long-term stability and high specific energy density, conducting 401.1 mAh g^{-1} (613.7 Wh kg^{-1}) at 0.5 A g^{-1} after 400 cycles. Xu et al. [122] successfully fabricated a hierarchical porous carbon (HPC) with inter-connected macro-pores and microporous shells using dual template method (Fig. 17). The HPC could provide a good conductive network, accommodate the volume change of pyrite FeS_2, and inhibit the growth of FeS_2 to get nano-sized FeS_2 particles as well as prohibit the loss of electroactive species through cycling. The as-prepared FeS_2@HPC structure showed enhanced electrochemical performance, a high specific capacity of 720 mAh g^{-1} could be obtained after 100 cycles, which is much higher than the capacity of pristine FeS_2.

Generally, one-dimensional (1D) nanostructures show unique properties, making them favorable to be used as active materials for LIBs. The application of 1D structured electrode materials owns many merits. Firstly, 1D structure allows the accommodation of the volume change of lithium insertion/extraction along a specific orientation. Secondly, the interval space formed between neighboring structures can act as a pathway for electrolyte, making diffusion of electrolyte into the inner region of the electrode easier, ultimately prolonging the lifespan of batteries. Thirdly, a much larger surface-to-volume ratio of 1D nanostructure arrays with respect to the bulk counterparts can provide more active sites and obviously shorten the diffusion route of Li ions [123]. Zhang et al. [124] prepared large-scale 1D FeS_2@C nanowires using organic-inorganic hybrid S-amine/FeS_2-amine (amine = ethylenediamine) (SAFA) nanowires. The FeS_2@C nanowires inherited the advantages of both 1D nanostructure and the thin amorphous carbon layers. Based on the merits of shortened Li ion diffusion distance,

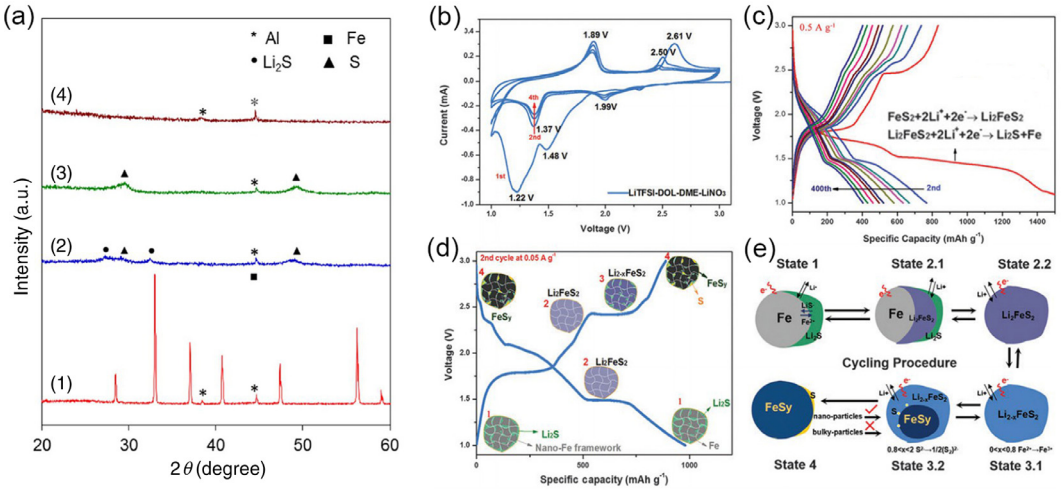


Fig. 16. (a) ex-situ XRD pattern of FeS_2 cathode at different cycling state: (1) pristine cathode, (2) after 1st discharging to 1.0 V, (3) after 1st recharging to 2.6 V, and (4) after 200 cycles at charged state (2.6 V). Reproduced with permission [111]. Copyright 2016, The Electrochemical Society. (b) Cyclic voltammetry curves (from 1st to 4th cycle at 0.2 mV s^{-1}), (c) cycling curves from the 2nd to the 100th cycle at 0.5 A g^{-1}, (d and e) schematic diagram for reaction mechanism. Reproduced with permission [120]. Copyright 2016, Royal Society of Chemistry.

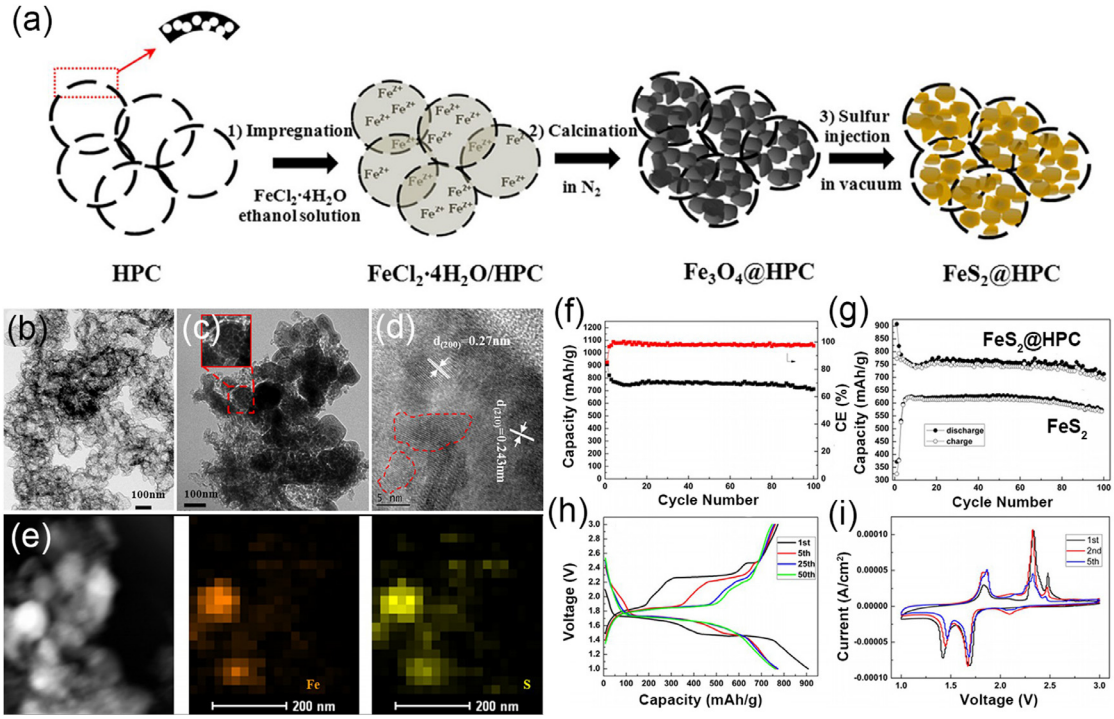


Fig. 17. (a) The formation process of FeS_2 nanocrystals in hierarchical porous carbon capsules. TEM images of (b) HPC and (c) FeS_2@HPC composite; (d) high-resolution TEM image; (e) scanning TEM image with phase mapping of the FeS_2@HPC composite. (f) Cycling performance and columbic efficiency (charge/discharge) of the FeS_2@HPC composite electrode at the rate of 1 C (1 C = 894 mA g^{-1}). (g) Charge and discharge curves of pristine FeS_2 and FeS_2@HPC. (h) Voltage profiles. (i) Cyclic voltammograms of FeS_2@HPC composite electrode. Reproduced with permission [122]. Copyright 2016, Elsevier.

improved electrical conductivity and precluded dissolution of polysulfides, the as-prepared FeS_2@C nanowires exhibited high reversible capacity up to 889 mAh g^{-1}. Excellent rate capability could be obtained, where the capacity could be maintained at 552 mAh g^{-1} at a high current density of 5 A g^{-1}. Additionally, superior cycling performance was manifested in FeS_2/Li batteries. After 100 cycles at a current density of 0.1 A g^{-1}, the reversible capacity of 570 mAh g^{-1} was kept with a Coulombic efficiency of over 98%. The self-supported hierarchical FeS_2/C composite nanotubes arrays were synthesized by a hydrolysis-sulfurization method, which was reported by Pan et al. [125]. The electrochemical performance of hierarchical FeS_2/C composite nanotubes was characterized by assembling FeS_2/Li batteries. The FeS_2/Li batteries showed noticeable improvement in the capacity, and the FeS_2/C nanotubes arrays showed initial specific capacity of 865 mAh g^{-1}, which was much higher than the bare FeS_2 electrodes. The rate performance of FeS_2/C nanotubes was also impressive, at a high rate of 1.5 C, and the capacity was 482 mAh g^{-1}. When the rate was changed to 0.25 C, the capacity could be go back to 721 mAh g^{-1}. Furthermore, superior cycling stability was obtained by the FeS_2/C nanotubes array. It showed a capacity of 689 mAh g^{-1} at 0.25 C and 390 mAh g^{-1}

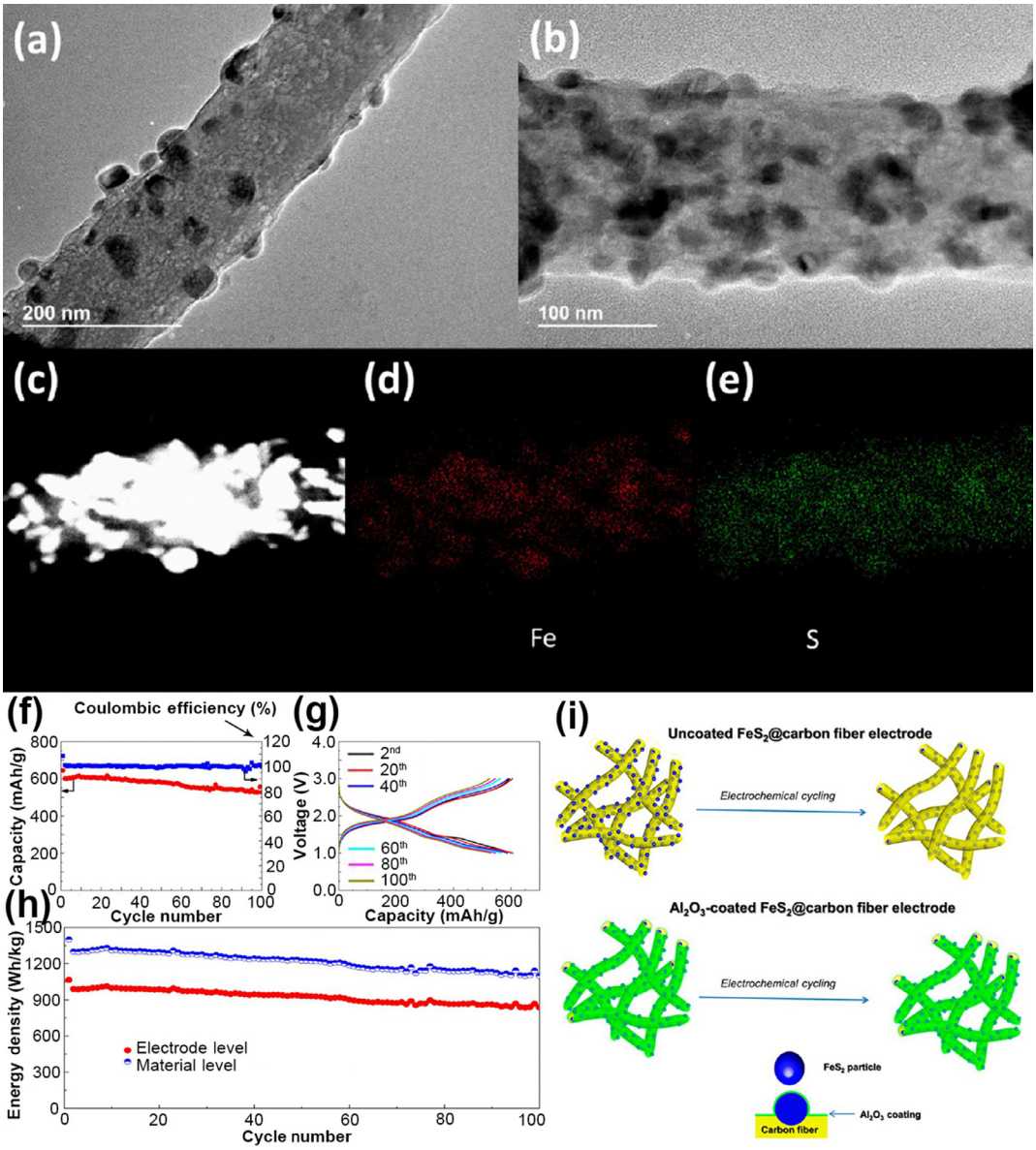


Fig. 18. (a–c) TEM images and EDS elemental mapping for (d) iron and (e) sulfur for the FeS_2@carbon fiber shown in (c). Electrochemical performance for the Al_2O_3-coated FeS_2@carbon fiber electrode tested in the solvent-in-salt electrolyte in the voltage range of 1.0~3.0 V (vs Li/Li^+). (f) Capacity retention test. (g) Lithiation – delithiation curves at different cycles. (h) Discharge energy density vs cycling number at the material level (~ Wh kg-FeS_2^{-1}) and the electrode level (~ Wh kg-FeS_2^{-1} electrode). (i) Schematic illustration of mechanisms for the enhanced cycling stability by Al_2O_3 coating in the voltage range of 1.0~3.0 V (vs Li/Li^+). Reproduced with permission [59]. Copyright 2016, American Chemical Society.

at 1.0 C after 100 cycles, respectively. In addition, the 3D structure of the electrode was basically maintained at 0.25 C after 100 cycles, indicating that the stable structure was favorable for achieving enhanced cycles. In the study by Zhu et al. [59], using an electrospinning method, an FeS_2@carbon fiber electrode was fabricated with FeS_2 nanoparticles either attached to or embedded in carbon fibers. By applying this free-standing FeS_2@carbon fiber electrode in FeS_2/Li batteries, the electrochemical performance and redox reaction mechanisms for the FeS_2/Li batteries were revealed (Fig. 18). The FeS_2@carbon fiber electrode showed stable electrochemical performance in both the solvent-in-salt-type Li-S battery electrolyte and the conventional carbonate-based electrolyte in the voltage range of 1.5~3.0 V. The authors concluded that after the charge-discharge process, the FeS_2/Li battery system transformed into a hybrid of a Li-FeS_2 and a Li-S system system. The improved electrochemical performance in the solvent-in-salt electrolyte compared with the carbonate electrolyte could be ascribed to the stabilized Li-S system performance using the solvent-in-salt electrolyte. By further coating a thin layer (~ 5 nm) of Al_2O_3 on the FeS_2@carbon fiber electrodes, the electrodes manifested improved electrochemical properties in the extended voltage range of 1.0~3.0 V. In this voltage range, the FeS_2@carbon fiber electrode showed a reversible capacity of 600 mAh g^{-1} (electrode) with an energy density reaching 1000 Wh kg^{-1} (electrode) and maintained at 840 Wh kg^{-1} (electrode) after 100 cycles, showing potential to be applied in energy storage system.

4.5. Other metal sulfides

Besides the above mentioned candidates, other TMSs, especially two-dimensional (2D) materials, such as TiS_2, WS_2 and VS_2, have

also been reported as promising anode for LIBs. Ti_2S is well-known as its high electronic/ionic conductivity, satisfying well with the demand of high-energy-density and high power. Therefore, many efforts have been paid since its proposal in 1970′s. Benefiting from the advantage of fast Li^+ diffusion rate, TiS_2 is mainly studied in high power batteries [126,127]. Lee et al. [128] demonstrated that TiS_2 was a suitable cathode material even in all-solid-state lithium battery. Constructing TiS_2 in all-solid state battery, the power density could reach the top of 1400 W Kg^{-1} at 10 C, and maintained over 1000 W kg^{-1} after 50 cycles. Like most other TMSs, the most challenging of TiS_2 is in-between voltage of 2.1 V vs. Li^+/Li. Finding suitable material to match with or new application system is viable strategy. For example, such voltage value is well stable in "Water-in-Salt" (WIS) electrolyte. Suo et al. [129] use TiS_2 as anode in WIS to pair with $LiMnO_2$ cathode. The result showed that the $LiMnO_2$/TiS_2 full cell could deliver energy density of 78 Wh kg^{-1} at a high discharge voltage of 1.7 V, revealing the possibility of using TiS_2 in WIS electrolyte LIB.

WS_2 is one of the two-dimensional layered transition-metal dichalcogenides. It has the same crystal structure as MoS_2, which possesses S-W-S layers through a van der Waals interaction. Such structure is favorite for Li^+ intercalation, promising its prospect application in energy storage. The semiconductor nature of reaction WS_2 and insulating nature of discharge products Li_2S lead to a slow kinetics. Therefore, many efforts have been made to improve the electric conductivity. The strategies, such as synthesizing mono- or few-layer WS_2, nanosized WS_2 and WS_2/C composites, have been put forward. Benefiting from its graphene-like structure, mono- or few-layer WS_2 usually exhibited outstanding electron transfer properties [130]. So far, various techniques have been developed, such as mechanical or chemical exfoliation [130–132]. Though monolayer WS_2 shows unique physiochemical properties, the high surface energy of WS_2 sheets makes them easy to restack. It is still challenging to fabricate stable mono- and few-layer with large scale. Besides, various morphologies, such as nanosheets [133], nanoflowers [134], nanotubes [135,136] have been synthesized. Benefiting from the large surface area and shorter Li^+ diffusion pathway of nanostructure, building nanostructure exhibited a promising strategy to enhance the Li^+ intercalation and deintercalation. Even though, the bulk WS_2 still suffers from low electron transfer. Adding additional carbon-based materials can significantly improve the conductivity of electrode material of WS_2. Recently, the studies showed that the combinations of nanostructure WS_2 and carbon-based materials could synergistically enhance the electrochemical performances of WS_2. Thus, a number of carbonaceous materials, such as graphene, CNTs, and amorphous carbon, have been reported to fabricate WS_2/C composites material [137–143]. For example, Zhang et al. [141] made the WS_2 nanosheets grown on graphene-wrapped carbon nanofibers (WS_2/GCNF). The obtained WS_2/GCNF possessed large surface area, high electrical conductivity and good structure integrity. As a result, the WS_2/GCNF exhibited high initial charge capacity of 1128.2 mAh g^{-1} at 100 mA g^{-1}, maintaining 95% capacity after 100 cycles. To simplify fabricating process, Wang et al. [142] utilized a simple solvothermal method and ice-template process to fabricate a hybrid nano-architecture composed of WS_2 nanosheets and CNT-rGO aerogel with microchannel three-dimensional (3D) scaffold structure. The WS_2 nanosheets had large surface area. The 3D structure not only provided excellent electronic pathway, but also great ionic channels. When acted as anode material for LIB, the WS_2/CNT-rGO could deliver a reversible capacity of 749 mAh g^{-1} at 100 mA g^{-1} with high initial Coulombic efficiency of 53.4%. Pang et al. [140] fabricated WS_2@CMK-3 nanocomposites through a one-step hydrothermal method. The CMK-3 had high electronic conductivity and volume confinement effect. Also, combined with the few-layered nanostructure of WS_2, the WS_2@CMK-3 maintained a high capacity of 720 mAh g^{-1} after 100 cycles at 100 mAh g^{-1}. Even at high current density of 2 A g^{-1}, a reversible capacity of 307 mAh g^{-1} could still be achieved.

The VS_2 is another 2D material, which is well known for its high rate performance as the electrode material for LIBs. But low discharge capacity was shown in the initial research. A breakthrough was made by Feng et al. [144], who obtained five S-V-S single layers by exfoliating bulk VS_2 flake, revealing the metallic nature of few-layered VS_2. Since then, much attention has been drawn to the mono- or few-layer VS_2. For example, utilizing the coincident interaction of VS_2 nanosheets with rGO, Fang et al. [145] synthesized VS_2/graphene nanosheets (VS_2/GNS), exhibiting excellent high-rate capability and great cycling stability. Even at 20 C, a high capacity of 114.2 mAh g^{-1} could still be obtained. Zhou et al. [146] prepared hierarchical VS_2 nanosheet assemblies, which consisted of ultrathin nanosheets with a few atomic layers thickness. The results showed that this unique structure enabled rapid and durable storage for alkali metal ions. When assembled as anode material for LIB, the reversible specific capacity could reach up to > 1000 mAh g^{-1}. Zhou et al. [147] prepared VS_4 nanoparticles rooted by amorphous carbon coated multi-walled carbon nanotubes via a simple solvothermal reaction. It delivered much better cycling stability and rate capability. It exhibited a reversible capacity of 922 mAh g^{-1} after cycled at 0.5 A g^{-1} for 100 times. Even after 1000 cycles at 2 or 5 A g^{-1}, it still delivered a capacity of 576 or 401 mAh g^{-1}. Apart from experiment data, recent first-principles calculations based on density functional theory also revealed that the 2D VS_2 monolayers could be the prospect anode materials for LIB, showing its promising application [148, 149].

5. Conclusions and perspectives

In summary, the review presents the recent advances in the modified TMSs for LIBs. The recent developments in structure and material design have made significant strides for LIBs, especially in the various structures of the carbon-based materials wrapped TMSs composites, which structures can solve the agglomeration and electrical conductivity issues of the TMSs. Furthermore, the carbon-based materials can also buffer the volume expansion and mitigate pulverization of the TMSs nanostructures during lithiation and de-lithiation processes. However, despite some significant strides have been achieved, the development of next-generation LIBs based on TMSs is still in its infancy, but the future outlook will be highlighted here.

In order to be practical, there are several issues that need to be further improved. First, there are some difficulties in the current methods of preparation. For example, the reaction process of the hydrothermal method is difficult to control and understand, the energy consumption of the microwave method is relatively high, and the efficiency and the yield of spray-related methods is not enough. Therefore, it is necessary to find a simple, low-cost and high-efficiency synthetic method for large-scale production of TMSs. In order to ensure the development of energy storage devices, the trend of using earth-abundant and non-toxic raw materials and green manufacturing processes has to be established without compromising on cost-effectiveness and environmental issues. Second, the ultimate goal of developing TMSs is to develop energy storage systems with high energy and power density. However, the energy density of a full battery depends on the operating voltage, in addition to the specific capacity of the positive and negative materials. Compared to the graphite anode, the voltage platform of TMSs is usually above 1.0 V, and therefore, it is a necessary to find a high-voltage cathode material that can match with TMSs to assemble a high voltage full battery. In addition, to match TMSs with the cathode material, the problem of compatibility with carbonate electrolytes needs to be addressed.

Acknowledgments

We gratefully acknowledge the financial support of the National Natural Science Foundation of China (21273185 and 21621091) and the National Found for Fostering Talents of Basic Science (J1310024). The authors also wish to express their thanks to Prof. D. W. Liao for his valuable suggestions.

References

[1] M.S. Whittingham, Chem. Rev. 104 (2004) 4271–4301.
[2] A.S. Arico, B.Scrosati P.Bruce, J.M. Tarascon, W.V. Schalkwijk, Nat. Mater 4 (2005) 366–377.
[3] M.V. Reddy, G.V. Subba Rao, B.V. Chowdari, Chem. Rev. 113 (2013) 5364–5457.
[4] C.H. Lai, M.Y. Lu, L.J. Chen, J. Mater. Chem. 22 (2012) 19–30.
[5] X. Rui, H. Tan, Q. Yan, Nanoscale 6 (2014) 9889–9924.
[6] X.Y. Yu, L. Yu, X.W.D. Lou, Adv. Energy Mater. 6 (2016) 1501333.
[7] T. Li, Q. Zhang, J. Energy Chem. 60 (2017) 1533–1539.
[8] H. Yuan, L. Kong, T. Li, Q. Zhang, Chin. Chem. Lett. 28 (2017) 2180–2194.
[9] M.R. Gao, Y.F. Xu, J. Jiang, S.H. Yu Chem, Soc. Rev. 42 (2013) 2986–3017.
[10] J. Cabana, L. Monconduit, D. Larcher, M.R. Palacin, Adv. Mater. 22 (2010) E170–E192.
[11] X. Xu, W. Liu, Y. Kim, J. Cho, Nano Today 9 (2014) 604–630.
[12] J.M. Yan, H.Z. Huang, J. Zhang, Z.J. Liu, Y. Yang, J. Power Sources 146 (2005) 264–269.
[13] G. Kalimuldina, I. Taniguchi, J. Mater. Chem. A 5 (2017) 6937–6946.
[14] S.S. Zhang, D.T. Tran, Electrochim. Acta 176 (2015) 784–789.
[15] Y. Shao-Horn, S. Osmialowski, Q.C. Horn, J. Electrochem. Soc. 149 (2002) A1547–A1555.
[16] U.K. Sen, P. Johari, S. Basu, C. Nayak, S. Mitra, Nanoscale 6 (2014) 10243–10254.
[17] N. Yamakawa, M. Jiang, C.P. Grey, Chem. Mater. 21 (2009) 3162–3176.
[18] J.S. Chung, H.J. Sohn, J. Power Sources 108 (2002) 226–231.
[19] A. Débart, L. Dupont, R. Patrice, J.M. Tarascon, Solid State Sci. 8 (2006) 640–651.
[20] B. Jache, B. Mogwitz, F. Klein, P. Adelhelm, J. Power Sources 247 (2014) 703–711.
[21] X. Li, X. He, C. Shi, B. Liu, Y. Zhang, S. Wu, Z. Zhu, J. Zhao, ChemSusChem 7 (2014) 3328–3333.
[22] M.T. McDowell, Z. Lu, K.J. Koski, J.H. Yu, G. Zheng, Y. Cui, Nano Lett. 15 (2015) 1264–1271.
[23] X. Wang, Y. Wang, X. Li, B. Liu, J. Zhao, J. Power Sources 281 (2015) 185–191.
[24] C. George, A.J. Morris, M.H. Modarres, M. De Volder, Chem. Mater. 28 (2016) 7304–7310.
[25] Q. Su, J. Xie, J. Zhang, Y. Zhong, G. Du, B. Xu, ACS Appl. Mater. Interf. 6 (2014) 3016–3022.
[26] Q. Su, G. Du, J. Zhang, Y. Zhong, B. Xu, Y. Yang, S. Neupane, K. Kadel, W. Li, ACS Nano 7 (2013) 11379–11387.
[27] C. Wang, S. Wang, L. Tang, Y.-B. He, L. Gan, J. Li, H. Du, B. Li, Z. Lin, F. Kang, Nano Energy 21 (2016) 133–144.
[28] X. Li, H.-C. Lin, W.-J. Cui, Q. Xiao, J.-B. Zhao, ACS Appl. Mater. Interf. 6 (2014) 7895–7901.
[29] G. Kalimuldina, I. Taniguchi, Electrochim. Acta 224 (2017) 329–336.
[30] F. Han, W. Li, D. Li, A Lu, ChemElectroChem 1 (2014) 733–740.
[31] C. Yu, Y. Wang, J. Zhang, W. Yang, X. Shu, Y. Qin, J. Cui, H. Zheng, Y. Zhang, P.M. Ajayan, Y. Wu, J. Power Sources 364 (2017) 400–409.
[32] Y. Xiao, J.Y. Hwang, I. Belharouak, Y.K. Sun, Nano Energy 32 (2017) 320–328.
[33] H. Zhou, Z. Lv, H. Liu, M. Liang, B. Liu, H. Guo, Electrochim. Acta 250 (2017) 376–383.
[34] D. Xie, X.H. Xia, W.J. Tang, Y. Zhong, Y.D. Wang, D.H. Wang, X.L. Wang, J.P. Tu, J. Mater. Chem. A 5 (2017) 7578–7585.
[35] S.Y. Lee, K.Y. Park, W.S. Kim, S. Yoon, S.H. Hong, K. Kang, M. Kim, Nano Energy 19 (2016) 234–245.
[36] S.B. Ranganath, A.S. Hassan, B.R. Ramachandran, C.D. Wick, J. Electrochem. Soc. 163 (2016) A2172–A2178.
[37] S.J. Rezvani, R. Gunnella, A. Witkowska, F. Mueller, M. Pasqualini, F. Nobili, S. Passerini, A.D. Cicco, ACS Appl. Mater. Interf. 9 (2017) 4570–4576.
[38] L. Yuan, X. Qiu, L. Chen, W. Zhu, J. Power Sources 189 (2009) 127–132.
[39] C. Feng, J. Ma, H. Li, R. Zeng, Z. Guo, H. Liu, Mater. Res. Bull. 44 (2009) 1811–1815.
[40] H. Hwang, H. Kim, J. Cho, Nano Lett. 11 (2011) 4826–4830.
[41] S. Ding, D. Zhang, J.S. Chen, X.W. Lou, Nanoscale 4 (2012) 95–98.
[42] Z. Wan, J. Shao, J. Yun, H. Zheng, T. Gao, M. Shen, Q. Qu, H. Zheng, Small 10 (2014) 4975–4981.
[43] K. Chang, W. Chen, ACS Nano 5 (2011) 4720–4728.
[44] J. Liu, A. Fu, Y. Wang, P. Guo, H. Feng, H. Li, X.S. Zhao, ChemElectroChem 4 (2017) 2027–2036.
[45] H. Li, K. Yu, H. Fu, B. Guo, X. Lei, Z. Zhu, J. Phys. Chem. C 119 (2015) 7959–7968.
[46] G.D. Stefanidis, A.N. Muñoz, G.S.J. Sturm, A. Stankiewicz, Rev. Chem. Eng. 30 (2014) 233–259.
[47] I. Bilecka, M. Niederberger, Nanoscale 2 (2010) 1358–1374.
[48] H. Li, Y. Wang, J. Huang, Y. Zhang, J. Zhao, Electrochim Acta 225 (2017) 443–451.
[49] N.H. Idris, M.M. Rahman, S.L. Chou, J.Z. Wang, D. Wexler, H.K. Liu, Electrochim. Acta 58 (2011) 456–462.
[50] S. Xiao, X. Li, W. Sun, B. Guan, Y. Wang, Chem. Eng. J. 306 (2016) 251–259.
[51] D.H. Youn, C. Jo, J.Y. Kim, J. Lee, J.S. Lee, J. Power Sources 295 (2015) 228–234.
[52] Y. Xiao, S.H. Lee, Y.-K. Sun, Adv. Energy Mater. 7 (2017) 1601329.
[53] G. Kalimuldina, I. Taniguchi, J. Solid State Electrochem. 21 (2017) 3057–3063.
[54] M.Y. Son, J.H. Choi, Y.C. Kang, J. Power Sources 251 (2014) 480–487.
[55] S.H. Choi, S.J. Boo, J.-H. Lee, Y.C. Kang, Sci. Rep. 4 (2014) 5755.
[56] H. Wang, S. Lu, Y. Chen, L. Han, J. Zhou, X. Wu, W. Qin, J. Mater. Chem. A 3 (2015) 23677–23683.
[57] S.C. Han, H.S. Kim, M.S. Song, J.H. Kim, H.J. Ahn, J.Y. Lee, J. Alloy Compd. 351 (2003) 273–278.
[58] T.A. Yersak, C. Stoldt, S.H. Lee, J. Electrochem. Soc. 160 (2013) A1009–A1015.
[59] Y. Zhu, X. Fan, L. Suo, C. Luo, T. Gao, C. Wang, ACS Nano 10 (2016) 1529–1538.
[60] L. Zhang, Y. Huang, Y. Zhang, H. Gu, W. Fan, T. Liu, Adv. Mater. Inter. 3 (2016) 1500467.
[61] Y.E. Miao, Y. Huang, L. Zhang, W. Fan, F. Lai, T. Liu, Nanoscale 7 (2015) 11093–11101.
[62] D.J. Chakrabarti, D.E. Laughlin, Bull. Alloy Phase Diag. 4 (1983) 254–271.
[63] J. Cheng, Y. Pan, J. Zhu, Z. Li, J. Pan, Z. Ma, J. Power Sources 257 (2014) 192–197.
[64] C. Feng, L. Zhang, Z. Wang, X. Song, K. Sun, F. Wu, G. Liu, J. Power Sources 269 (2014) 550–555.
[65] M. Zhou, N. Peng, Z. Liu, Y. Xi, H. He, Y. Xia, Z. Liu, S. Okada, J. Power Sources 306 (2016) 408–412.
[66] H. Li, H. Zhou, Chem. Commun. 48 (2012) 1201–1217.
[67] H.C. Tao, X.L. Yang, L.L. Zhang, S.B. Ni, J. Phys. Chem. Solids 75 (2014) 1205–1209.
[68] D. Yuan, G. Huang, F. Zhang, D. Yin, L. Wang, Electrochim Acta 203 (2016) 238–245.
[69] Y. Wang, Y. Zhang, H. Li, Y. Peng, J. Li, J. Wang, B.J. Hwang, J. Zhao, Chem. Eng. J. 332 (2018) 49–56.
[70] Y. Liu, B. Jin, Y.F. Zhu, X.Z. Ma, X.Y. Lang, Int. J. Hydrogen Energy 40 (2015) 670–674.
[71] X. Meng, S.C. Riha, J.A. Libera, Q. Wu, H.H. Wang, A.B.F. Martinson, J.W. Elam, J. Power Sources 280 (2015) 621–629.
[72] Y. Zhang, K. Li, Y. Wang, J. Zeng, P. Ji, J. Zhao, Mater. Sci. Eng. B 213 (2016) 57–62.
[73] Y. Wang, H. Li, Y. Zhang, Y. Peng, P. Zhang, J. Zhao, Nano Res. (2017) 1–14.
[74] Y. Wang, Y. Zhang, H. Li, Y. Peng, J. Li, J. Wang, B.J. Hwang, J. Zhao, Electrochim. Acta 247 (2017) 271–280.
[75] J. Wang, S.H. Ng, G.X. Wang, J. Chen, L. Zhao, Y. Chen, H.K. Liu, J. Power Sources 159 (2006) 287–290.
[76] Q. Wang, L. Jiao, Y. Han, H. Du, W. Peng, Q. Huan, D. Song, Y. Si, Y. Wang, H. Yuan, J. Phys. Chem. C 115 (2011) 8300–8304.
[77] J. Ge, Y. Li, Chem. Commun. 19 (2003) 2498–2499.
[78] Z. Wang, L. Pan, H. Hu, S. Zhao, CrystEngComm 12 (2010) 1899–1904.
[79] B.S. Geller, Acta Cryst. 15 (1962) 1195–1198.
[80] R. Jin, J. Liu, Y. Xu, G. Li, G. Chen, J. Mater. Chem. A 1 (2013) 7995–7999.
[81] X. Zhang, H. Wang, G. Wang, J Colloid Interf. Sci 492 (2017) 41–50.
[82] J. Liu, C. Wu, D. Xiao, P. Kopold, L. Gu, P.A. van Aken, J. Maier, Y. Yu, Small 12 (2016) 2354–2364.
[83] G. Qu, H. Geng, D. Ge, M. Tang, J. Zheng, H. Gu, Electrochim. Acta 211 (2016) 305–312.
[84] Y. Zhou, D. Yan, H. Xu, S. Liu, J. Yang, Y. Qian, Nanoscale 7 (2015) 3520–3525.
[85] S. Liu, J. Wang, J. Wang, F. Zhang, L. Wang, Appl. Surface Sci. 390 (2016) 86–91.
[86] P. Zeng, J. Li, M. Ye, K. Zhuo, Z. Fang, Chemistry 23 (2017) 9517–9524.
[87] R. Jin, J. Zhou, Y. Guan, H. Liu, G. Chen, J. Mater. Chem. A, 2 (2014) 13241–13244.
[88] P. Long, Z. Zhang, G. Peng, Q. Zhang, D. Liu, X. Xu, X. Yao, New J. Chem. 41 (2017) 9184–9191.
[89] Y. Zhou, D. Yan, H. Xu, J. Feng, X. Jiang, J. Yue, J. Yang, Y. Qian, Nano Energy 12 (2015) 528–537.
[90] G.D.Q. Su, J. Zhang, Y. Zhong, B. Xu, Y. Yang, S. Neupane, K. Kadel, W. Li, ACS Nano 7 (2013) 11379–11387.
[91] H. Wang, J. Ma, S. Liu, L. Nie, Y. Chai, X. Yang, R. Yuan, J. Alloys Compd. 676 (2016) 551–556.
[92] Y. Tan, M. Liang, P. Lou, Z. Cui, X. Guo, W. Sun, X. Yu, ACS Appl. Mater. Interf. 8 (2016) 14488–14493.
[93] C. Wu, J. Maier, Y. Yu, Adv. Mater. 28 (2016) 174–180.
[94] C. Xu, Y. Jing, J. He, K. Zhou, Y. Chen, Q. Li, J. Lin, W. Zhang, J. Alloys Compd. 708 (2017) 1178–1183.
[95] J. Zhang, L. Yu, X.W.D. Lou, Nano Res. 10 (2017) 4298–4304.
[96] J. He, Y. Chen, P. Li, F. Fu, Z. Wang, W. Zhang, Electrochim. Acta 182 (2015) 424–429.
[97] S. Tao, W. Huang, H. Xie, J. Zhang, Z. Wang, W. Chu, B. Qian, L. Song, RSC Adv. 7 (2017) 39427–39433.
[98] J. Guo, F. Li, Y. Sun, X. Zhang, L. Tang, Electrochim. Acta 167 (2015) 32–38.
[99] B. Qiu, X. Zhao, D. Xia, J. Alloys Compd. 579 (2013) 372–376.
[100] W. Chen, T. Li, Q. Hu, C. Li, H. Guo, J. Power Sources 286 (2015) 159–165.
[101] Q. Wang, R. Zou, W. Xia, J. Ma, B. Qiu, A. Mahmood, R. Zhao, Y. Yang, D. Xia, Q. Xu, Small 11 (2015) 2511–2517.
[102] L. Yu, J.F. Yang, X.W. Lou, Angew. Chem. 55 (2016) 13422–13426.
[103] Q. Su, J. Xie, J. Zhang, Y. Zhong, G. Du, B. Xu, ACS Appl. Mater. Interf. 6 (2014) 3016–3022.

[104] X.Y. Yu, L. Yu, X.W.D. Lou, Small Methods 1 (2017) 1600020.
[105] Y. Wang, L. Yu, X.W.D. Lou, Angew. Chem. Int. Ed. 55 (2016) 7423–7426.
[106] T. Stephenson, Z. Li, B. Olsen, D. Mitlin, Energy Environ. Sci. 7 (2014) 209–231.
[107] X. Fang, C. Hua, X. Guo, Y. Hu, Z. Wang, X. Gao, F. Wu, J. Wang, L. Chen, Electrochim. Acta 81 (2012) 155–160.
[108] X. Wang, D.M Tang, H. Li, W. Yi, T. Zhai, Y. Bando, D. Golberg, Chem. Commun. 48 (2012) 4812–4814.
[109] S.C. Han, K.W. Kim, H.J. Ahn, J.H. Ahn, J.Y. Lee, J. Alloys Compd. 361 (2003) 247–251.
[110] G. Kalimuldina, I. Taniguchi, J. Mater. Chem. A 5 (2017) 6937–6946.
[111] S.S. Zhang, D.T. Tran, J. Electrochem. Soc. 163 (2016) A792–A797.
[112] J. Xiao, X. Wang, X.Q. Yang, S. Xun, G. Liu, P.K. Koech, J. Liu, J.P. Lemmon, Adv. Funct. Mater. 21 (2011) 2840–2846.
[113] X.Y. Yu, H. Hu, Y. Wang, H. Chen, X.W. Lou, Angew. Chem. Int. Ed. 54 (2015) 7395–7398.
[114] M. Chhowalla, H.S. Shin, G. Eda, L.-J. Li, K.P. Loh, H. Zhang, Nat. Chem. 5 (2013) 263.
[115] X. Wang, G. Li, M.H. Seo, F.M. Hassan, M.A. Hoque, Z. Chen, Adv. Energy Mater. 5 (2015) 1501106.
[116] H. Jiang, D. Ren, H. Wang, Y. Hu, S. Guo, H. Yuan, P. Hu, L. Zhang, C. Li, Adv. Mater. 27 (2015) 3687–3695.
[117] H.H. Fan, H.H. Li, K.C. Huang, C.Y. Fan, X.Y. Zhang, X.L. Wu, J.P. Zhang, ACS Appl. Mater. Interf. 9 (2017) 10708–10716.
[118] W. Huang, S. Li, X. Cao, C. Hou, Z. Zhang, J. Feng, L. Ci, P. Si, Q. Chi, ACS Sustain. Chem. Eng. 5 (2017) 5039–5048.
[119] R. Fong, J.R. Dahn, C.H.W. Jones, J. Electrochem. Soc. 136 (1989) 3206–3210.
[120] S.B. Son, T.A. Yersak, D.M. Piper, S.C. Kim, C.S. Kang, J.S. Cho, S.S. Suh, Y.U. Kim, K.H. Oh, S.H. Lee, Adv. Energy Mater. 4 (2014) 1300961.
[121] R. Tan, J. Yang, J. Hu, K. Wang, Y. Zhao, F. Pan, Chem. Commun. 52 (2016) 986–989.
[122] X. Xu, T. Cai, Z. Meng, H. Ying, Y. Xie, X. Zhu, W.-Q. Han, J. Power Sources 331 (2016) 366–372.
[123] J. Jiang, Y. Li, J. Liu, X. Huang, Nanoscale 3 (2011) 45–58.
[124] F. Zhang, C. Wang, G. Huang, D. Yin, L. Wang, J. Power Sources 328 (2016) 56–64.
[125] G.X. Pan, F. Cao, X.H. Xia, Y.J. Zhang, J. Power Sources 332 (2016) 383–388.
[126] A. Samad, A. Shafique, Y.H. Shin, Nanotechnology 28 (2017) 175401.
[127] Rudolf Winter, P. Heitjans, J. Phys. Chem. B 105 (2001) 6108–6115.
[128] JamesE. Trevey, ConradR. Stoldt, S.-H. Lee, J. Electrochem. Soc. 158 (2011) A1282–A1289.
[129] W. Sun, L. Suo, F. Wang, N. Eidson, C. Yang, F. Han, Z. Ma, T. Gao, M. Zhu, C. Wang, Electrochem. Commun. 82 (2017) 71–74.
[130] B. Radisavljevic, A. Radenovic, J. Brivio, V. Giacometti, A. Kis, Nat. Nanotechnol. 6 (2011) 147–150.
[131] G. Eda, H. Yamaguchi, D. Voiry, T. Fujita, M. Chen, M. Chhowalla, Nano Lett. 11 (2011) 5111–5116.
[132] J.N. Coleman, M. Lotya, A. 'Neill, S.D. Bergin, P.J. King, U. Khan, K. Young, A. Gaucher, S. De, R.J. Smith, I.V. Shvets, S.K. Arora, G. Stanton, H.Y. Kim, K. Lee, G.T. Kim, G.S. Duesberg, T. Hallam, J.J. Boland, J.J. Wang, J.F. Donegan, J.C. Grunlan, G. Moriarty, A. Shmeliov, R.J. Nicholls, J.M. Perkins, E.M. Grieveson, K. Theuwissen, D.W. McComb, P.D. Nellist, V. Nicolosi, Science 331 (2011) 568–571.
[133] J.W. Seo, Y.W. Jun, S.W. Park, H. Nah, T. Moon, B. Park, J.G. Kim, Y.J. Kim, J. Cheon, Angew. Chem. Int. Ed. Engl. 46 (2007) 8828–8831.
[134] A. Prabakaran, F. Dillon, J. Melbourne, L. Jones, R.J. Nicholls, P. Holdway, J. Britton, A.A. Koos, A. Crossley, P.D. Nellist, N. Grobert, Chem. Commun. 50 (2014) 12360–12362.
[135] A Rothschild, G.L. Frey, M. Homyonfer, R. Tenne, M. Rappaport, Mater. Res. Innoat. 3 (1999) 145–149.
[136] A. Zak, L. Sallacan-Ecker, A. Margolin, Y. Feldman, R. Popovitz-Biro, A. Albu–Yaron, M. Genut, R. Tenne, Fuller. Sci. Technol. 19 (2010) 18–26.
[137] Z. Yuan, Q. Jiang, C. Feng, X.Z. Chen, S.J. Guo, Electron. Mater. (2017) 568–571.
[138] S. Liu, B. Shen, Y. Niu, M. Xu, J. Colloid Interf. Sci. 488 (2017) 20–25.
[139] T. Wang, C. Sun, M. Yang, L. Zhang, Y. Shao, Y. Wu, X. Hao, Electrochim. Acta 259 (2018) 1–8.
[140] Q. Pang, Y. Gao, Y. Zhao, Y. Ju, H. Qiu, Y. Wei, B. Liu, B. Zou, F. Du, G. Chen, Chemistry 23 (2017) 7074–7080.
[141] L. Zhang, W. Fan, T. Liu, Nanoscale 8 (2016) 16387–16394.
[142] Y. Wang, D. Kong, W. Shi, B. Liu, G.J. Sim, Q. Ge, H.Y. Yang, Adv. Energy Mater. 6 (2016) 1601057.
[143] J. Zou, C. Liu, Z. Yang, C. Qi, X. Wang, Q. Qiao, X. Wu, T. Ren, ChemElectroChem 4 (2017) 2232–2236.
[144] J. Feng, X. Sun, C. Wu, L. Peng, C. Lin, S. Hu, J. Yang, Y. Xie, J. Am. Chem. Soc. 133 (2011) 17832–17838.
[145] W. Fang, H. Zhao, Y. Xie, J. Fang, J. Xu, Z. Chen, ACS Appl. Mater. Interf. 7 (2015) 13044–13052.
[146] R. Sun, Q. Wei, J. Sheng, C. Shi, Q. An, S. Liu, L. Mai, Nano Energy 35 (2017) 396–404.
[147] Y. Zhou, J. Tian, H. Xu, J. Yang, Y. Qian, Energy Storage Mater. 6 (2017) 149–156.
[148] D. Wang, Y. Liu, X. Meng, Y. Wei, Y. Zhao, Q. Pang, G. Chen, T J. Mater. Chem. A 5 (2017) 21370–21377.
[149] N.S. Mikhaleva, M.A. Visotin, A.A. Kuzubov, Z.I. Popov, J. Phys. Chem. C 121 (2017) 24179–24184.